Mon. Not. R. Astron. Soc. **000**, 000–000 (2001) Printed 1 February 2008 (MN LATEX style file v1.4)

# Mass segregation in young compact star clusters in the Large Magellanic Cloud: I. Data and Luminosity Functions

R. de Grijs⋆, R.A. Johnson†, G.F. Gilmore and C.M. Frayn
*Institute of Astronomy, University of Cambridge, Madingley Road, Cambridge CB3 0HA*



Accepted —. Received —; in original form —.

**ABSTRACT**

We have undertaken a detailed analysis of *HST/WFPC2* and STIS imaging observations, and of supplementary wide-field ground-based observations obtained with the NTT of two young ($\sim 10-25$ Myr) compact star clusters in the LMC, NGC 1805 and NGC 1818. The ultimate goal of our work is to improve our understanding of the degree of primordial mass segregation in star clusters. This is crucial for the interpretation of observational luminosity functions (LFs) in terms of the initial mass function (IMF), and for constraining the universality of the IMF.

We present evidence for strong luminosity segregation in both clusters. The LF slopes steepen with cluster radius; in both NGC 1805 and NGC 1818 the LF slopes reach a stable level well beyond the clusters' core or half-light radii. In addition, the brightest cluster stars are strongly concentrated within the inner $\sim 4R_{\rm hl}$.

The global cluster LF, although strongly nonlinear, is fairly well approximated by the core or half-light LF; the (annular) LFs at these radii are dominated by the segregated high-luminosity stars, however.

We present tentative evidence for the presence of an excess number of bright stars surrounding NGC 1818, for which we argue that they are most likely massive stars that have been collisionally ejected from the cluster core. We therefore suggest that the cores of massive young stars clusters undergo significant dynamical evolution, even on time-scales as short as $\sim 25$ Myr.

**Key words:** stars: luminosity function, mass function – galaxies: star clusters – Magellanic Clouds – globular clusters: individual: NGC 1805, NGC 1818

## 1 INTRODUCTION: MASS SEGREGATION AND ITS IMPLICATIONS

One of the major uncertainties in modern astrophysics is the issue of whether the stellar initial mass function (IMF) is universal or, alternatively, determined by environmental effects. Galactic globular clusters (GCs) and rich, compact Magellanic Cloud star clusters are ideal laboratories for providing strong constraints on the universality of the IMF, in particular because they are essentially single age, single metallicity systems for which statistically significant samples of individual stars over a range of masses can easily be resolved.

However, the effects of mass segregation in both young and old star clusters, in the sense that the more massive stars are more centrally concentrated than the lower-mass stars, clearly complicate the interpretation of an observed luminosity function (LF) at a given position within a star cluster in terms of its IMF. Without reliable corrections for the effects of mass segregation, hence for the structure and dynamical evolution of the cluster, it is impossible to obtain an accurate estimate of the IMF from the observational LF.

In this paper, we will concentrate on the analysis of the behaviour of the stellar LF of two young Large Magellanic Cloud (LMC) star clusters as a function of radius; in a companion paper (de Grijs et al. 2001, Paper II), we will derive the associated mass functions (MFs) and discuss in detail how this transformation depends on the assumed models. Finally, in a forthcoming paper (de Grijs et al., in prep., Paper III), we will extend our analysis to our larger LMC cluster sample, spanning a significant age range, in which we will attempt to model the dynamical cluster evolution.

Although the standard picture, in which stars in dense clusters evolve rapidly towards a state of energy equipartition through stellar encounters, with the corresponding mass segregation, is generally accepted, observations of various

⋆ E-mail: grijs@ast.cam.ac.uk
† Present address: European Southern Observatory, Alonso de Cordova 3107, Santiago 19, Chile

degrees of mass segregation in very young star clusters (e.g., Hillenbrand 1997, Testi et al. 1997, Fischer et al. 1998, Hillenbrand & Hartmann 1998, Hillenbrand & Carpenter 2000) suggest that at least some of this effect is related to the process of star and star cluster formation itself (cf. Paper II): these clusters are often significantly younger than their two-body relaxation time (even the equivalent relaxation time in the core), the time scale on which dynamical mass segregation should occur. Quantifying the degree of actual mass segregation is thus crucial for the interpretation of observational LFs in terms of the IMF, even for very young star clusters.

Although dynamical two-body relaxation effects tend to segregate a cluster's mass distribution roughly on its mean relaxation time scale, possibly enhanced by some degree of primordial mass segregation, the observability of mass segregation depends on a number of conditions. These are mostly interrelated and include, among others, the cluster's degree of central concentration, its age, the radial range sampled by the observations and, most of all, the observer's ability to resolve the individual cluster stars towards the cluster centre. *Hubble Space Telescope (HST)* observations show, almost without exception, mass segregation effects in old Galactic GCs, in rich, compact Magellanic Cloud clusters, and in young star clusters still embedded in molecular clouds, although to varying degrees. Not surprisingly, the fraction of ground-based observations reporting the detection of mass segregation effects, sometimes even in the same objects, is significantly lower. We will now briefly discuss the observational evidence for mass segregation in the youngest star clusters.

### 1.1 Rich Compact Magellanic Cloud Clusters

Since the rich, compact star clusters in the Magellanic Clouds span a wide range of ages, from $\sim 10^6$ to $\sim 1.3\times10^{10}$ yr (cf. Elson & Fall 1988), observable effects of mass segregation due to two-body relaxation need not be expected *a priori*, particularly for the youngest clusters. Ground-based observations may be severely hampered by crowding in the cluster cores, thus hiding possible signatures of dynamical, as well as primordial, mass segregation. This is likely the case in a number of the young star clusters in the LMC studied by Elson, Fall & Freeman (1987) and Subramaniam, Sagar & Bhatt (1993), although the uncertainties in the power-law slopes of the MFs derived by Elson et al. (1987), down to a given limiting brightness, are large and could possibly hide mass segregation signatures.

The quality of ground-based data for rich LMC clusters often allows only marginal confirmation of possible mass segregation effects, especially in young clusters if based on LF differences as a function of cluster radius (e.g., NGC 1711, Subramaniam et al. 1993; NGC 1866, Elson et al. 1987). Similarly, ground-based observations of H4 (Mateo & Hodge 1986), LW 79 (Mateo & Hodge 1987), and ESO121-SC09 (Mateo, Hodge & Schommer 1986, Papenhausen & Schommer 1988) report either no convincing (LW 79) or marginal evidence for mass segregation based on the distributions of main-sequence and giant-branch stars, due to small-number statistics in the cluster cores.

In all other LMC clusters studied for this purpose to date, using either LFs or their associated MFs as a function of radius to assess the distributions of stars of varying brightness (mass), ground-based observations (e.g., NGC 2100, Westerlund 1961; NGC 2098 and SL 666, Kontizas et al. 1998) do indeed show strong indications of mass segregation. In addition, observations with the *HST* have also resulted in convincing cases for mass segregation, e.g., in all objects in our own LMC cluster sample (cf. Elson et al. 1999 for NGC 1868, and Santiago et al. 2001; hereafter SBJG), in NGC 2157 (Fischer et al. 1998), and in the Small Magellanic Cloud (SMC) star cluster NGC 330 (Sirianni et al. 2001). The results of SBJG were based on a first, preliminary analysis of the *WFPC2* observations also used in this paper. Here, we present a more detailed analysis of the effects of luminosity segregation in the two youngest clusters in our LMC sample, while combining the *WFPC2* data with the STIS observations also obtained as part of the same programme (cf. Section 2), and with wide-field ground-based observations obtained with the NTT.

We note that for one of the objects in our sample, NGC 1818, contradicting results have been obtained: Hunter et al. (1997) did not find evidence for mass segregation in this cluster for stellar masses in the range $0.85 \leq m \leq 9M_\odot$, with the proviso that the cluster core does contain brighter stars that were not included in their study due to saturation, whereas the outer regions do not. Recently, however, SBJG confirmed significant mass segregation, based on the radial variance of the cluster LFs. Elson et al. (1998) adopted a different approach, and concluded that the fraction of binary stars increases significantly from $\sim 20\%$ in the outer regions to $\sim 35\%$ in the core. This is consistent with expectations from *(i)* dynamical mass segregation, where we might expect the more massive binaries to have undergone substantial two-body relaxation while single stars would not have (cf. Paper II), and *(ii)* the radial dependence of the binary creation and destruction rates in these young star clusters. Elson et al. (1998) show that their derived IMF is fully consistent with Hunter et al.'s (1997) results.

### 1.2 Very Young Star Clusters

The study of proto-stellar clusters, i.e., very young associations of stars still embedded in the molecular clouds from which they originated, might give us a handle to constrain the degree of primordial mass segregation. In the Galaxy, in three such young star clusters (YSCs) mass segregation effects have been studied in detail in the past decade.

Ground-based observations of both NGC 2024 (Lada et al. 1991, Carpenter et al. 1997) and the Monoceros R2 (MonR2) complex (Carpenter et al. 1997) have not been able to show the presence or absence of (possibly primordial) mass segregation convincingly. While Lada et al. (1991) suggested that the brighter stars in NGC 2024 seem to be more centrally concentrated than the fainter cluster members, this evidence was deemed inconclusive by Carpenter et al. (1997). They argued that this result was based on an incomplete sample of cluster stars, although mass segregation might be limited to the OB stars forming in the very centre. These same authors argued that for masses below $2M_\odot$, mass segregation effects in MonR2 amount to only a $\sim 2\sigma$ result, although the most massive star ($\sim 10M_\odot$) appears to be forming near the cluster centre, where their extinction-limited sample of cluster stars does not reach.

A combination of both ground-based (e.g., Hillenbrand 1997) and *HST* observations (e.g., Hillenbrand & Hartmann 1998) of the Orion Nebula Cluster (ONC), and in particular of its very core, the Trapezium stars, have presented clear evidence for mass segregation for the $m > 5M_{\odot}$ component, with some evidence for general mass segregation down to $m \simeq 1$–$2M_{\odot}$ (Hillenbrand & Hartmann 1998, see also the review by Larson 1993). Mass segregation in this YSC has, in fact, been known for more than 5 decades, as pointed out by Hillenbrand & Hartmann (1998).

Finally, R136, the central cluster in the actively star-forming 30 Doradus region in the LMC (age $\lesssim$ 3–4 Myr, cf. Hunter et al. 1995), has been studied extensively, both from the ground and with *HST*. A variety of techniques have revealed a significant overabundance of high-mass stars in its very centre, and thus strong mass segregation (e.g., Campbell et al. 1992, Larson 1993, Malumuth & Heap 1994, Brandl et al. 1996). Hunter et al. (1995) constrained the central region in which possible mass segregation effects were observed to $r \lesssim 0.5$ pc, and found little evidence of mass segregation beyond this radius for stars in the mass range $2.8 \leq m \leq 15M_{\odot}$. However, they reported a hint of an excess of bright stars within 0.5 pc, and a deficit of the highest-mass stars in the annulus $0.6 \leq r \leq 1.2$ pc, which would be consistent with expectations for mass segregation. Brandl, Chernoff & Moffat (2001), finally, present very interesting evidence for the ejection of a fair number of massive stars from the core, due to two-body encounters, which could not, with higher confidence, be attributed to alternative scenarios.

Thus, in most of the young compact star clusters that can be resolved in individual stars by currently available telescopes, mass segregation effects are observed, *although to varying degrees*. This underlines the importance of our understanding of the physical processes involved in the formation and evolution of star clusters, and in particular of the IMF, which will ultimately determine whether a young star cluster will eventually be destroyed or evolve to a Galactic GC-type object.

Because of their large range in ages, rich compact star clusters in the LMC are ideal candidates to assess the effects and magnitude of dynamical mass segregation, provided that one can constrain the degree of primordial mass segregation to within reasonable uncertainties. Constraining this degree of primordial mass segregation is of crucial importance to discriminate among different theories of star formation in clusters, which generally depend on the presence of extensive dissipation processes. The presence or absence of dissipation during the star formation process may have significantly different effects on the radial dependence of the IMF (cf. Fischer et al. 1998).

## 2 THE LMC CLUSTER SAMPLE

In this paper, we will focus on the two youngest LMC star clusters in our sample, NGC 1805 and NGC 1818. Table 1 contains the current best estimates available in the literature for a few of the most important properties of each cluster, including their age, metallicity, core radii, mass, adopted distance modulus, foreground reddening E($B$–$V$), and median relaxation time-scale. For a full overview of the clusters' physical parameters, we refer the reader to `http://www.ast.cam.ac.uk/STELLARPOPS/LMCdatabase/`.

**Table 1.** Fundamental parameters of NGC 1805 and NGC 1818

| | NGC 1805 | Ref. | NGC1818 | Ref. |
|---|---|---|---|---|
| log( age ) [yr] | 7.0 ± 0.05 | 1,8 | 7.2 ± 0.1 | 1,5,8 |
| | | | 7.41 | 1 |
| [Fe/H] (dex) | ∼ 0.0 | 6 | ∼ 0.0 | 6 |
| | | | −0.4 | 6[a] |
| E($B-V$) (mag) | 0.04 | 2 | 0.03 | 2 |
| | | | 0.05 | 5 |
| $(m-M)_0$ (mag) | 18.59 | 2 | 18.58 | 2 |
| $R_{\rm core}$ (pc)[c] | 1.39 | 9 | 2.1 ± 0.4 | 4 |
| | | | 2.56 | 9 |
| $R_{\rm hl}$ (pc)[c] | 1.8 | 7 | 2.6 | 7 |
| log( $t_{\rm rh}$)[b] [yr] | ... | | 9.0 – 9.7 | 3 |
| Mass ($M_{\odot}$) | $0.6 \times 10^4$ | 6 | $3 \times 10^4$ | 5 |
| Centre (J2000) | RA = 05 02 05 | 9 | RA = 05 04 03 | 9 |
| (RA: hh mm ss; | Dec = −66 06.7 | 9 | Dec = −66 26.0 | 9 |
| Dec: dd mm.m) | | | | |

NOTES:
[a] best estimate from measurements in the literature
[b] depending on the mass-to-light ratio assumed
[c] based on $(m-M)_{0,\rm LMC} = 18.5$, or $D_{\rm LMC} = 52$ kpc.

REFERENCES: 1 – Cassatella et al. (1996); 2 – Castro et al. (2001); 3 – Elson, Fall & Freeman (1987a); 4 – Elson, Freeman & Lauer (1989); 5 – Hunter et al. (1997); 6 – Johnson et al. (2001); 7 – Santiago et al. (2001); 8 – Santos, Jr., et al. (1995); 9 – this paper.

### 2.1 Observations

To study the effects of mass segregation properly, the observational data needs to meet the following conditions:

(i) The observability of the effects of *dynamical* mass segregation is a strong function of a cluster's age (cf. Paper II) and the observer's ability to resolve individual stars, in particular in its core. Due to crowding, the observations in the core need to be of high resolution.

(ii) Since the initial mass of stars at the main sequence turn-off magnitude and the mass of stars on the giant and horizontal branches is approximately constant, we will need to obtain deep observations, extending well down the main sequence, in order to sample a sufficiently large mass range. In fact, as Bolte (1989) argued, since the dynamical relaxation time scale for the cluster stars, with the exception of those in the very core, is long compared to the time scale for mass loss between the main sequence and horizontal branch, we can in principle extend our analysis to include stars from the horizontal branch down to the completeness limit of the main sequence.

As part of *HST* GO programme 7307, we obtained *WFPC2* and STIS imaging observations of the populous LMC clusters in Table 1. The high resolution of the *WFPC2*/PC observations ($\sim$ 1.8 pixels; the pixel size of the WF chips is $0.097''$, with a total combined field of view of roughly 4850 arcsec$^2$ for the entire *WFPC2* detector, while the PC pixel size is $0.0455''$) meets the first condition above, while the deep STIS data allow for the construction of very deep LFs down to $\sim 0.2M_{\odot}$; in fact, STIS (in imaging mode through long-pass [LP] filters) is five times more sensitive for faint red objects than *WFPC2*.

Although parts of the observations of the LMC clusters have been described elsewhere already (e.g., Beaulieu

et al. 1999, Elson et al. 1999, Castro et al. 2001, Johnson et al. 2001, SBJG), here we will give a brief overview of the available data for the two youngest star clusters in our sample. This paper builds on the preparatory research by SBJG, which we will continue in significantly greater detail; colour-magnitude diagrams (CMDs) of these clusters were published by Johnson et al. (2001). These latter authors focused predominantly on the brighter stars in NGC 1805 and NGC 1818 to consider ages and age ranges. In this study we include the entire range of magnitudes down to the 50% completeness limit (Sec. 2.6) to consider the evidence for luminosity and mass segregation in these clusters.

#### *2.1.1 WFPC2 observations*

We obtained *WFPC2* exposures through the F555W and F814W filters (roughly corresponding to the Johnson-Cousins $V$ and $I$ filters, resp.) for each cluster, with the PC centred on both the cluster centre, and on its half-mass radius. Following SBJG, we will refer to these two sets of exposures as our CEN and HALF fields, respectively. For the CEN fields, we obtained both deep (exposure times of 140s and 300s, respectively, for each individual image in F555W and F814W) and shallow (exposure times of 5s and 20s were used for the F555W and F814W filters, respectively) images. The shallow exposures were intended to obtain aperture photometry for the brightest stars in the cluster centres, which are saturated in the deeper exposures. At each position, for each set of deep and shallow exposures, and through both filters, we imaged our clusters in sets of 3 individual observations, to facilitate the removal of cosmic rays (Sec. 2.2). For the HALF field, we obtained deep observations with a total exposure time of 2500s through each filter. The saturation level for all of the individual calibrated observations, as used in our subsequent analysis, is roughly 3600 counts. A summary of our CEN and HALF *WFPC2* observations is included in Table 2. In Fig. 1 we show the composite (combined CEN and HALF fields) *WFPC2* F555W images of the two clusters.

Note the small subcluster $\sim 90''$ (22 pc) South East of NGC 1818; this is cluster NGC 1818 B (cf. Will et al. 1995, Grebel 1997), located at RA(J2000) = 05:04:01.82; Dec (J2000) = −66:26:46.1. NGC 1818 B is found to be of similar age, $\sim 30$ Myr, as NGC 1818 (Grebel 1997), although it is not clear whether NGC 1818 B is associated with NGC 1818. The configuration of both clusters is reminiscent of the LMC cluster pair NGC 1850 and NGC 1850 A, which are apparently physically associated with each other (cf. Caloi & Cassatella 1998).

In addition, parallel *WFPC2* fields, located $\sim 7'$ from each cluster centre, were obtained with NICMOS as primary detector. These fields, with total exposure times (two images combined) of 1200s and 800s for F555W and F814W, respectively, will be used for the subtraction of the background LMC field stars and unresolved background galaxies (Sec. 3; cf. Castro et al. 2001, SBJG). We will refer to these fields as "NGC 1805-par" and "NGC 1818-par", respectively. In addition, we also obtained deeper *WFPC2* observations of a background field ("Background-1"), with exposure times of 7800s and 5200s in F555W and F814W, respectively. This field was selected to represent the faint LMC disk background at a similar distance from the bar to the clusters of interest here.

The *WFPC2* results presented in this paper are based on an independent reprocessing of the data used by SBJG (using slightly different methods) as a check that the results are not sensitive to the data reduction techniques applied.

#### *2.1.2 STIS imaging observations*

We also obtained deep STIS CCD observations of small sections of the cluster HALF fields in ACCUM imaging mode through the F28×50LP filter. The fields were exposed for 2950s each in sets of 5 observations (see also Elson et al. 1999; Table 2); each observation was split into 2 exposures to allow for the removal of cosmic rays by the data processing pipeline. The STIS CCD covers a nominal $52'' \times 52''$ square field of view, with $1024 \times 1024 \sim 0.05''$ pixels. The actual field of view of our combined HALF fields measures $48 \times 28''$, for both clusters.

#### *2.1.3 Wide-field ground-based observations*

Finally, we obtained wide-field ground-based observations of both LMC clusters with the ESO New Technology Telescope (NTT) at La Silla, Chile, equipped with the EMMI wide field imager. These observations were obtained in service mode on 1 September 2000 using the standard $V$ (#606), and $I$ (#610) filters under photometric conditions (see Table 2 for the observational characteristics); the seeing FWHM for these observations ranged roughly between 0.8 and $1.0''$. We used EMMI's red Tektronix TK2048 EB Grade 2 CCD, #36, with a pixel size of $0.27''$ and a field of view of $9.15' \times 8.6'$. The data were reduced following standard reduction procedures; calibration solutions were obtained by using stars in common between the NTT and *WFPC2* fields.

### 2.2 Image Processing

Pipeline image reduction and recalibration of the *WFPC2* and STIS images was done with standard procedures provided as part of the IRAF/STSDAS[‡] package, using the updated and corrected on-orbit flat fields and related reference files most appropriate for our observations.

Since our *WFPC2* images with a common pointing were aligned to within a few hundredths of a pixel, we simply coadded the individual observations in a given filter for each of the CEN or HALF fields using the IRAF task CRREJ to improve the signal-to-noise ratio in our images. This task also removed cosmic ray events in a series of iterations that allow correction for cosmic ray hits in pixels adjacent to those that already have been corrected in an earlier iteration. After some experimenting, we found that as few as 3 iterations

[‡] The Image Reduction and Analysis Facility (IRAF) is distributed by the National Optical Astronomy Observatories, which is operated by the Association of Universities for Research in Astronomy, Inc., under cooperative agreement with the National Science Foundation. STSDAS, the Space Telescope Science Data Analysis System, contains tasks complementary to the existing IRAF tasks. We used Version 2.2 (August 2000) for the data reduction performed in this paper.

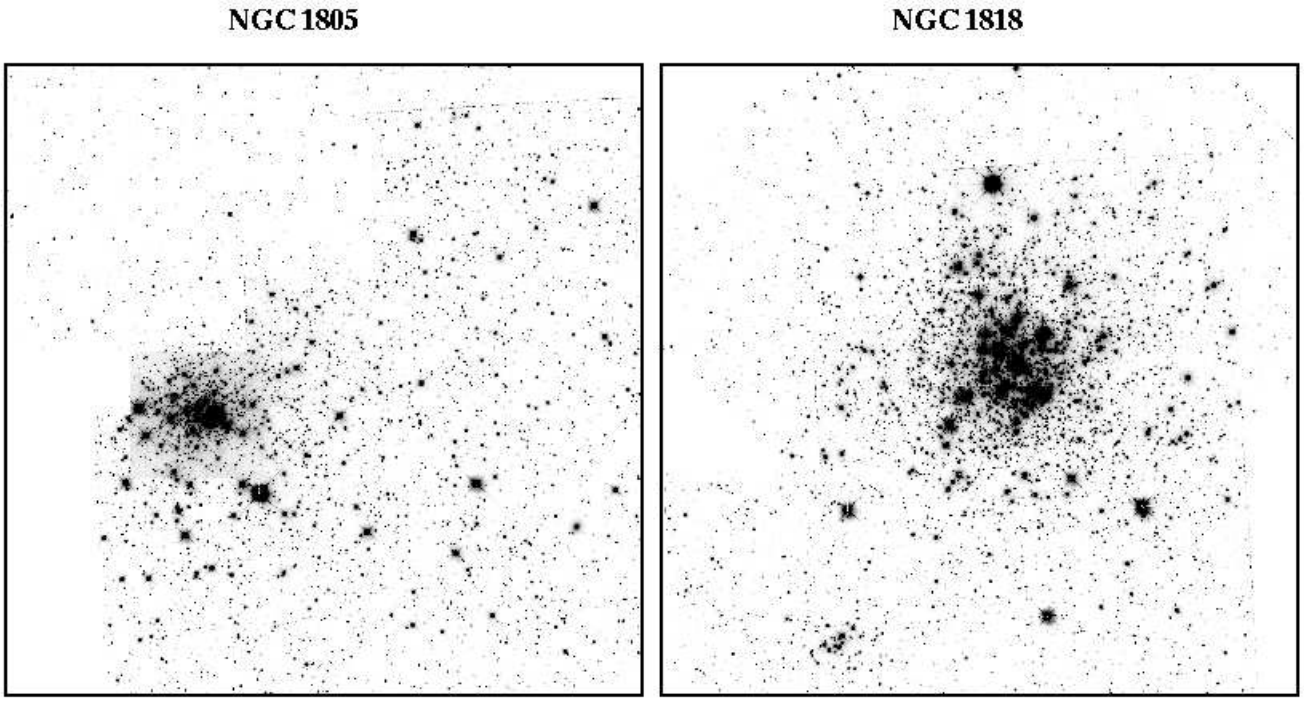


**Figure 1.** Combined CEN and HALF *WFPC2* F555W images of NGC 1805 and NGC 1818. Each panel is $164 \times 164''$ ($\sim 41 \times 41$ pc); North is up, East to the left. For reasons of clarity and dynamic range, the central cluster regions are represented by the PC fields of view of the 3x140s CEN exposures, since they are mostly saturated in the HALF fields.

produce output images in which the remaining cosmic ray hits – if any – are indistinguishable from poisson noise. We carefully checked that the corruption of the centres of the brighter stars in our images by the cosmic ray rejection routines, due to slight misalignments among the 3 individual exposures, was kept to a minimum by comparing the results of aperture photometry before and after combining our science exposures.

Alignment of the individual recalibrated STIS images was ensured by running IRAF's IMALIGN task (requiring shifts of $\lesssim 2$ pixels in either direction), upon which a median-filtered final image was produced using the IMCOMBINE task.

We used the final images for each of the cluster fields and for each filter to obtain source lists (Sec. 2.3) and to subsequently perform aperture photometry on these source lists (Sec. 2.4).

### 2.3 Source Selection

We based our initial selection of source candidates on a modified version of the DAOFIND task in the DAOPHOT software package (Stetson 1987), running under IDL.[§]

For both the CEN and HALF fields, we decided to combine and cross-correlate the source lists obtained in both the F555W and F814W passbands to define our master source lists, for each cluster field. We allowed only a 1-pixel positional mismatch between the individual source detections in F555W and F814W. After some experimenting, we decided to set our detection thresholds at four times the appropriate sky background noise level ($\sigma_{\rm bg}$) in each of our final *WFPC2* images. This turned out to be the best compromise between including the maximum number of genuine source detections and the minimum number of spurious features due to noise or artifacts along diffraction spikes of bright saturated stars in the fields.

The automated source detection routine, used with suitable constraints on source sharpness and roundness parameters, and the subsequent cross-correlation technique resulted in combined source lists largely devoid of non-stellar objects and saturated stars, thus minimising potential contamination of our photometry. However, to prevent contamination by background galaxies or possibly remaining instrumental artifacts, we employed a second size selection criterion to our master source lists, using a Gaussian fitting routine to estimate source extent. Although the *WFPC2* PSF is decidedly non-Gaussian, this technique, when applied uniformly to all objects, provides a fairly accurate assessment of the relative object sizes, thus allowing us to distinguish between stars and non-stellar objects. Measurements of stars in our

[§] The Interactive Data Language (IDL) is licensed by Research Systems Inc., of Boulder, CO.

**Table 2.** Overview of the observations

| Object | Field | Detector | Filter | Exposure time (s) | RA[a] (J2000) | Dec[a] (J2000) | Position angle (°)[b] | Date (UT) (dd/mm/yyyy) |
|---|---|---|---|---|---|---|---|---|
| NGC 1805 | CEN | *WFPC2* | F555W | 3x5 | 05:02:21.652 | −66:06:43.110 | −89.88 | 25/07/1998 |
| | | | | 3x140 | | | | |
| | | | F814W | 3x20 | | | | 25/07/1998 |
| | | | | 3x300 | | | | |
| | HALF | | F555W | 2x800 | 05:02:24.533 | −66:06:12.752 | −177.09 | 29/04/1998 |
| | | | | 900 | | | | |
| | | | F814W | 3x800 | | | | 28/04/1998 |
| | | | | 900 | | | | |
| | | STIS | F28x50LP | 5x2950 | 05:02:24.668 | −66:06:14.190 | 53.06 | 13/03/1998 |
| | Wide | NTT | $V_{606}$[c] | 3x60 | 05:04:13.9 | −66:26:05.5 | 88.50 | 10/01/2000 |
| | | | | 2x20 | | | | |
| | | | $I_{610}$[c] | 3x60 | 05:04:13.9 | −66:26:05.5 | 88.50 | 10/01/2000 |
| | | | | 2x10 | | | | |
| NGC 1818 | CEN | *WFPC2* | F555W | 3x5 | 05:04:14.135 | −66:26:05.647 | −45.09 | 25/09/1998 |
| | | | | 3x140 | | | | |
| | | | F814W | 3x20 | | | | 25/09/1998 |
| | | | | 3x300 | | | | |
| | HALF | | F555W | 2x800 | 05:04:12.261 | −66:26:33.152 | −177.09 | 30/04/1998 |
| | | | | 900 | | | | |
| | | | F814W | 3x800 | | | | 30/04/1998 |
| | | | | 900 | | | | |
| | | STIS | F28x50LP | 5x2950 | 05:04:12.345 | −66:26:34.081 | 167.06 | 29/07/1998 |
| | Wide | NTT | $V_{606}$[c] | 4x60 | 05:04:13.9 | −66:26:05.5 | 88.50 | 10/01/2000 |
| | | | | 2x20 | | | | |
| | | | $I_{610}$[c] | 3x60 | 05:04:13.9 | −66:26:05.5 | 88.50 | 10/01/2000 |
| | | | | 2x10 | | | | |
| | | | | Background fields | | | | |
| NGC 1805-par | | *WFPC2* | F555W | 2x600 | 05:01:28.193 | −66:01:04.943 | 44.72 | 08/12/1997 |
| | | | F814W | 2x400 | | | | 08/12/1997 |
| | | STIS | F28x50LP | 2x1350 | 05:02:22.939 | −65:57:07.421 | −34.94 | 08/12/1997 |
| NGC 1818-par | | *WFPC2* | F555W | 2x600 | 05:03:24.113 | −66:20:04.149 | 48.81 | 11/12/1997 |
| | | | F814W | 2x400 | | | | 11/12/1997 |
| | | STIS | F28x50LP | 2x1350 | 05:03:18.941 | −66:19:12.111 | −69.73 | 05/12/1997 |
| Background-1 | | *WFPC2* | F555W | 6x1300 | 05:11:27.853 | −65:29:01.693 | −72.00 | 13/08/1998 |
| | | | F814W | 4x1300 | | | | 26/08/1998 |

[a] For *WFPC2*, centre of the PC; for STIS observations, field centre; for NTT observations, telescope pointing; [b] East w.r.t. North; [c] These are filter names in the NTT nomenclature, and not related to *HST* filter names.

images, and comparison with both stars from the *WFPC2* PSF library and artificial PSFs produced by Tiny Tim (Krist & Hook 1997), showed that the Gaussian $\sigma$ of the *WFPC2* PSF profile is of order 0.80–0.85 WF or PC pixels; we therefore only retained sources with $0.55 \leq \sigma_{\rm Gauss} \leq 1.15$, thus allowing for the non-Gaussian PSF shape and for effects of instrumental noise on the measured sizes, in particular of the fainter objects. We are very confident that our final source lists thus obtained exclusively contain genuine stars.

For the STIS images, we also employed a 4 $\sigma_{\rm bg}$ detection limit and similar final source list selection techniques.

The total numbers of genuine stars for each cluster field are listed in Table 3.

### 2.4 Aperture Photometry

Because of the undersampling of point sources by the *WFPC2* optics, aperture photometry produces more accurate magnitude and colour measurements than PSF fitting, in not too crowded fields (cf. Castro et al. 2001, SBJG). Therefore, we obtained aperture photometry of the stars in our final source lists, using 2-pixel aperture radii. This corresponds to 0.2″ radii for the 3 WF chips and $r = 0.09''$ for the PC. A 2-pixel aperture radius is close to the optimum radius for stellar aperture photometry in rich star clusters; it produces the smallest photometric errors and the narrowest main sequence for our sample clusters. It is a compromise between the need to include the core of the PSF but avoid light contamination by neighbouring objects.

In addition, to avoid runaway photometric errors due to steep gradients in the background light because of nearby bright stars or diffraction spikes, we included a criterion to reject sources with mode(background) > (background $+25 \times \sigma_{\rm bg}$). Extensive experimentation showed that this rejection limit only excluded objects for which the photometry was genuinely affected by nearby bright or saturated stars. The number of stars rejected at this stage is also listed in Table 3. The relatively large number of rejected sources in the HALF fields of either cluster is due to fact that the parts of the cluster centres imaged by these exposures contain a large number of bright, saturated stars (due to the long exposure times), in the vicinity of which the photometric errors are unacceptably large.

Significant aperture corrections (ACs), determined from the individual data frames, were then applied to the measured magnitudes. For the individual *WFPC2* chips, we used the position-dependent ACs to 0.5″ apertures used by Johnson et al. (2001), defined as $\mathrm{AC} = a + b\,r_c$, where $r_c$ is the distance from the centre of the chip in pixels. These ACs were found to be the same for the short and long CEN exposures, as well as for the HALF and parallel (background) fields taken close in time. For the STIS fields, we used a single AC for each of our cluster fields, which we found to

**Table 3.** Source detections and saturation levels

| Object | Field | Instrument | Filter | # Stars (total) | # Rej.[a] | Saturation level (mag)[b] |
|---|---|---|---|---|---|---|
| NGC 1805 | CEN | *WFPC2* | F555W | 5457 | 10 | 15.5, 18.6 |
| | | | F814W | 5457 | 62 | 15.5, 18.6 |
| | HALF | | F555W | 5850 | 173 | 20.6 |
| | | | F814W | 5850 | 127 | 20.5 |
| | All | | | 10202 | | |
| | HALF | STIS | F28x50LP | 612 | 16 | 18.0 |
| | Wide | NTT | $V_{606}$ | 2000 | 35 | 15.5 |
| | | | $I_{610}$ | 2000 | 21 | 15.6 |
| NGC 1818 | CEN | *WFPC2* | F555W | 6881 | 25 | 15.0, 18.3 |
| | | | F814W | 6881 | 62 | 15.0, 18.4 |
| | HALF | | F555W | 7368 | 823 | 20.5 |
| | | | F814W | 7368 | 606 | 20.4 |
| | All | | | 12833 | | |
| | HALF | STIS | F28x50LP | 896 | 5 | 18.0 |
| | Wide | NTT | $V_{606}$ | 2371 | 117 | 15.5 |
| | | | $I_{610}$ | 2371 | 108 | 15.6 |
| | | | Background fields | | | |
| NGC 1805-par | | *WFPC2* | F555W | | | 20.3 |
| | | | F814W | | | 20.0 |
| NGC 1818-par | | | F555W | | | 20.3 |
| | | | F814W | | | 20.0 |
| Background-1 | | | F555W | | | 22.0 |
| | | | F814W | | | 21.5 |

Notes: [a] This refers to the number of stars rejected from the final sources lists due to abnormally high background levels, or steep background gradients due to the vicinity of saturated stars; CEN: long exposures only; [b] CEN exposures: short, long.

**Table 4.** Aperture corrections to 0.5″ apertures.

| Object | Filter | Chip | $a$ | $b$ | |
|---|---|---|---|---|---|
| NGC 1805 | F555W | PC | 0.3174 | 1.13 | $\times10^{-4}$ |
| | | WF2 | 0.1511 | 7.6783 | $\times10^{-5}$ |
| | | WF3 | 0.1811 | 6.6327 | $\times10^{-5}$ |
| | | WF4 | 0.1488 | 1.0811 | $\times10^{-4}$ |
| | F814W | PC | 0.5071 | 1.95 | $\times10^{-4}$ |
| | | WF2 | 0.1797 | 8.0328 | $\times10^{-5}$ |
| | | WF3 | 0.2116 | 3.0135 | $\times10^{-5}$ |
| | | WF4 | 0.1829 | 8.7969 | $\times10^{-5}$ |
| | F28x50LP | STIS | 0.468 | | |
| NGC 1818 | F555W | PC | 0.3192 | 1.098 | $\times10^{-4}$ |
| | | WF2 | 0.1276 | 1.3832 | $\times10^{-4}$ |
| | | WF3 | 0.2020 | 9.9948 | $\times10^{-6}$ |
| | | WF4 | 0.1424 | 1.3596 | $\times10^{-4}$ |
| | F814W | PC | 0.5469 | 8.9871 | $\times10^{-5}$ |
| | | WF2 | 0.1959 | 9.8792 | $\times10^{-5}$ |
| | | WF3 | 0.2562 | 2.2080 | $\times10^{-5}$ |
| | | WF4 | 0.2088 | 1.0289 | $\times10^{-4}$ |
| | F28x50LP | STIS | 0.463 | | |

be very similar to those obtained by Houdashelt, Wyse & Gilmore (2001). We list our aperture corrections in Table 4.

Before applying these corrections, however, we first corrected the aperture magnitudes for the geometric distortion of the *WFPC2* chips, using the correction equations from Holtzman et al. (1995a), and then for the time-dependent charge transfer (in)efficiency (CTE) determined by Whitmore, Heyer & Casertano (1999).

### 2.5 Photometric Calibration

#### *2.5.1 WFPC2 photometry*

We used the transformation coefficients of Holtzman et al. (1995a) to convert the aperture-corrected *WFPC2* photometry to the standard Johnson-Cousins *V, I* photometric system:

$$\begin{aligned} V &= -2.5\times\log\dot{C}(\mathrm{F555W}) + (-0.052\pm0.007)\times(V-I) \\ &+ (0.027\pm0.002)\times(V-I)^2 + (21.725\pm0.005) \\ &+ 2.5\times\log(\mathrm{GR})\,, \end{aligned} \quad (1)$$

and

$$\begin{aligned} I &= -2.5\times\log\dot{C}(\mathrm{F814W}) + (-0.062\pm0.009)\times(V-I) \\ &+ (0.025\pm0.002)\times(V-I)^2 + (20.839\pm0.006) \\ &+ 2.5\times\log(\mathrm{GR})\,. \end{aligned} \quad (2)$$

Here, $\dot{C}$ is the count rate in 0.″5 apertures, and GR is the gain ratio as defined by Holtzman et al. (1995b), which accounts for the difference in gain states between calibration and science observations. For *WFPC2* in its state with an analog-to-digital gain of 7 electrons (bay 4; as for our observations) GR is 1.987, 2.003, 2.006 and 1.955 for the PC, WF2, WF3 and WF4 chips, respectively, subject to an $\sim 1\%$ uncertainty. These transformations hold for $-0.3 < (V-I) < 1.5$, which covers most of the colour range of the stars in our LMC clusters. The colour terms in Eqs. (1) and (2) are defined in the standard system; consequently, the equations must be applied iteratively to measures from the *WFPC2* frames.

We found a small offset between source magnitudes from the long and short CEN exposures (cf. Johnson et al. 2001). Since the main purpose of the short CEN exposures was to obtain reliable magnitudes for the brightest stars populating the cluster LFs, we applied a simple magnitude offset to the short exposures. These offsets, which we have listed in Table 5, were determined over the common range of magnitudes in the short and long exposures with similar measurement uncertainties (based on the appearance of their CMDs), i.e. in the range $18.6 \leq \mathrm{mag} \leq 20.0$ and $18.4 \leq \mathrm{mag} \leq 19.8$ for NGC 1805 and NGC 1818, respectively, for both *V* and *I*. Since they were determined inde-

**Table 5.** Photometric offsets applied to match the photometry of exposures with different exposure times.

| Object | Filter | Chip | mag(long) – mag(short) | mag(CEN) – mag(HALF) |
|---|---|---|---|---|
| NGC 1805 | F555W | PC | 0.072 ± 0.074 | |
| | | WF2 | 0.031 ± 0.099 | |
| | | WF3 | 0.044 ± 0.111 | |
| | | WF4 | 0.050 ± 0.124 | |
| | | All | | −0.027 ± 0.053 |
| | F814W | PC | 0.064 ± 0.047 | |
| | | WF2 | −0.011 ± 0.042 | |
| | | WF3 | −0.009 ± 0.053 | |
| | | WF4 | 0.004 ± 0.080 | |
| | | All | | −0.094 ± 0.063 |
| NGC 1818 | F555W | PC | 0.069 ± 0.060 | |
| | | WF2 | 0.041 ± 0.065 | |
| | | WF3 | 0.030 ± 0.048 | |
| | | WF4 | 0.041 ± 0.069 | |
| | | All | | 0.016 ± 0.092 |
| | F814W | PC | 0.052 ± 0.053 | |
| | | WF2 | 0.028 ± 0.050 | |
| | | WF3 | 0.017 ± 0.050 | |
| | | WF4 | 0.024 ± 0.056 | |
| | | All | | 0.063 ± 0.150 |

pendently, and using a different method of analysis, small differences between our and Johnson et al.'s (2001) offsets occur, although not in a systematic way. This lends additional credibility to our photometry.

At this point, we combined the master source lists obtained from the CEN long and short exposures, and subsequentially the lists from the combined CEN exposures and the HALF fields. The merging of the short and long CEN exposures was based on the following considerations:

(i) If both long and short magnitudes are available for a particular object, use the long exposures, but only if $V_{\rm long} > V_{\rm sat.,long}$ *and* $I_{\rm long} > I_{\rm sat.,long}$, where the subscript "sat.,long" indicates the saturation limit of the long exposures (Table 3). Otherwise, use the short exposures, but only if the observations are not saturated in at least one passband.

(ii) If only magnitudes from the long exposures are available for the object, use these if the observations are not saturated in at least one passband.

(iii) If only short-exposure magnitudes are available, use these if either $V_{\rm short} < V_{\rm sat.,long}$ or $I_{\rm short} < I_{\rm sat.,long}$, *and* the observations are not saturated in at least one passband.

Before combining the CEN and HALF field detections, we also needed to correct the HALF exposures for the small photometric offset found for matching sources in the CEN fields; the corresponding offsets are also listed in Table 5. The subsequent merging of the CEN and HALF fields was done largely along similar lines:

(i) If only magnitudes from the combined CEN list are available, keep these.

(ii) If both CEN and HALF magnitudes were determined, keep the CEN magnitude if it is brighter than $V = 23.0$ and $I = 23.5$; otherwise use the HALF data.

(iii) If only a HALF-field detection was registered, keep this if the object is not saturated in at least one passband.

Finally, we corrected our photometry for the effects of Galactic foreground extinction using the extinction values tabulated in Table 1. Most of these values were derived from isochrone fits to the clusters' CMDs (Castro et al. 2001, SBJG). We determined the extinction in the *HST* passbands assuming the Galactic extinction law of Rieke & Lebofsky (1985), convolved with the *HST* filter shapes, $A_{\rm F555W}/A_V = 1.081$ and $A_{\rm F814W}/A_V = 0.480$ (de Grijs et al. 2001). One should be cautious to apply an extinction estimate for a non-standard bandpass, which is then subsequently transformed to a standard magnitude. For NGC 1805, however, the difference in the extinction correction between the F555W and $V$-band filters is negligible for practical purposes, namely $\leq 0.010$ mag, while for the F814W/$I$ band this reduces to $A_I - A_{\rm F814W} \leq 0.001$ mag. The equivalent extinction differences for NGC 1818 are $\leq 0.007$ and $\leq 0.001$ mag, respectively.

### *2.5.2 STIS photometry*

To convert our STIS LP magnitudes to the standard $V$ magnitudes, we first transformed them to *WFPC2* flight system magnitudes using the empirical transformations obtained by Beaulieu et al. (2001) for STIS CCD observations with analog-to-digital gain 4 (as for our observations):

$$\begin{aligned} V_{555} &= 23.473 - 2.5 \times \log \dot{C} - 0.5184 \times (V_{555} - I_{814}) \\ &- 0.0502 \times (V_{555} - I_{814})^2 , \end{aligned} \quad (3)$$

and subsequently used the standard *WFPC2*-to-ground transformations to obtain standard $V$ magnitudes (cf. Holtzman et al. 1995a). The STIS-to-$V_{555}$ transformation was derived for the Galactic GC NGC 6553 ([Fe/H] $\approx -0.2$) for magnitudes determined in $0.5''$ apertures, and are valid for sources with $1.8 \lesssim (V_{555} - I_{814}) \lesssim 4$.

Houdashelt et al. (2001) also obtained empirical transformations between STIS LP and *WFPC2* flight magnitudes, based on the Galactic GCs 47 Tuc ([Fe/H] $\sim -0.7$) and M15 ([Fe/H] $\sim -2.2$), using the F606W and F814W *WFPC2* filters. They concluded that – if quadratic transformations are assumed (as in Beaulieu et al. 2001) – there is no evidence for a metallicity dependence in the transformation relations. Their transformation equations apply to the entire $(V_{606} - I_{814})$ colour range covered by their observations, i.e. $0.35 \lesssim (V_{606} - I_{814}) \lesssim 1.85$, which translates to $-0.1 \lesssim (V_{555} - I_{814}) \lesssim 1.4$ for stellar spectral types in the range from early B to G, which is based on the folding of synthetic spectra through the filter bandpasses using the SYNPHOT package in IRAF.

Since a significant number of the STIS-detected sources did not have counterparts with well-determined magnitudes in either the F555W or F814W images, we assumed all sources in the final STIS source list to be cluster stars and approximated their $(V_{555} - I_{814})$ colours to be those of the main sequence stars of the appropriate magnitude determined from our *WFPC2* CMDs.

To correct for foreground extinction, we used the extinction correction obtained by Beaulieu et al. (2001), $A_{V_{\rm LP}} = 2.505 E(B-V)$, which is based on integration across the passband.

## 2.6 Completeness

Due to the significant stellar density gradient across the cluster fields, completeness corrections are a strong function of

position within a cluster. Therefore, we computed completeness corrections for all observations in circular annuli around the centre of each cluster, for both the PC and the WF fields, located at intervals between the centre and $3.6''$, $3.6-7.2''$, $7.2-18.0''$, $18.0-36.0''$, $36.0-54.0''$ and at radii $\geq 54.0''$. At the distance of the LMC, $1''$ corresponds to $\sim 0.25$ pc. The cluster centre coordinates, included in Table 1, were determined by smoothing the cluster light distributions and subsequently applying an ellipse-fitting routine to the smoothed cluster profiles.

We added an area-dependent number of Gaussian sources to the individual annuli, ranging from $\sim 60$ in the inner annulus to 2000 in the outer, partial annulus. We created artificial source fields for input magnitudes between 15.0 and 27.0 mag, in steps of 0.5 mag. Their $(V-I)$ colours were distributed following the clusters' main sequence ridge lines, i.e., they were magnitude dependent. We then applied the same source detection routines to the fields containing the combined cluster stars and the artificial sources. The results of this exercise, based on the long CEN exposures, are shown in Fig. 2. These completeness curves were corrected for the effects of blending or superposition of multiple randomly placed artificial stars as well as for the superposition of artificial stars on genuine objects. Due to the large number of bright, saturated stars in the innermost annulus of NGC 1805, proper completeness tests could not be done in this area; for comparison, we have plotted the corresponding completeness curve in this area for the short CEN exposures instead. The progressive increase in completeness fraction with radius for a given source brightness clearly illustrates the potentially serious effects of crowding in the inner regions of the clusters. In the analysis performed in this paper, we only include those ranges of the stellar LF where the completeness fraction is in excess of 50%.

As mentioned in Sec. 2.3, the *HST* PSF is non-Gaussian in shape. Therefore, we have introduced an additional uncertainty by adding Gaussian-shaped artificial objects to our science frames for the completeness analysis. A detailed comparison of the light profiles of the Gaussian sources on the one hand and PSFs from the *WFPC2* PSF library and Tiny Tim artificial PSFs on the other, reveals that, except for the innermost pixel, both light profiles closely match each other. Since our source detection routine requires information on both the brightness *and* the shape of the objects in order to include them, and because for those magnitudes where the incompleteness becomes significant source detections are photon noise limited and therefore relatively independent of the stellar profile shape, we estimate that by using Gaussian light profiles, we will have obtained *conservative* completeness estimates. In other words, for any given magnitude range, we may have obtained completeness fractions that are marginally too low, and would need to be shifted to slightly fainter magnitudes ($\ll 0.5$ mag).

We also determined completeness curves for the background fields. Thanks to their low stellar density, a single completeness curve for the WF chips was found to apply to any one background field, as shown in Fig. 3. The higher resolution obtained with the PC translates into a greater completeness fraction compared to the WF chips. The completeness curves for the NGC 1805-par and NGC 1818-par fields are identical, within the observational uncertainties.

Finally, we applied the same analysis to the STIS science frames and background fields, using a single completeness curve for the entire STIS field of view. The 50% completeness limit occurs at $V_{555} \simeq 25$ and $\simeq 24.5$ in NGC 1805 and NGC 1818, respectively, for the science frames and – due to their shorter exposure times – roughly 0.2–0.3 mag brighter in the parallel background fields.

## 3 APPROACH: DATA PREPARATION AND LUMINOSITY FUNCTIONS

In this section, we will examine the dependence of the shape and slope of the stellar LF on position within the clusters. We basically use the cluster LFs as smoothing functions of the full two-dimensional (*V, V–I*) CMDs. The full *N*-body modeling of the cluster CMDs, fully inclusive of the latest input physics (e.g., binary star mergers), *except the effects of mass segregation*, was discussed by Johnson et al. (2001) and shown to represent the observed CMDs very well. Where the full 2-dimensional CMDs were used to infer the presence and the effects of mass segregation, this was mostly based on differences in the concentration of specific stellar types, most often main sequence and giant branch stars, in young LMC clusters (cf. Sect. 1.1) and old GCs (e.g., in NGC 1851, Saviane et al. 1998; NGC 5466, Nemec & Harris 1987; Pal 12, Harris & Canterna 1980; and 47 Tuc, Da Costa 1982). However, our cluster stars start to saturate at the faint end of the red giant branch, so this approach is not feasible. In fact, with the exception of a handful of the brightest stars, we are limited to the analysis of the main sequence stars in these clusters (cf. the CMDs in Johnson et al. 2001).

In order to study the positional dependence of the LF within our star clusters, we need to correct the observed stellar LFs in the CEN and HALF fields for the contribution of stars from the galactic (LMC) background in these fields. For that purpose, we obtained the background field LFs using identical procedures as for the CEN and HALF fields themselves. The resulting LFs are statistically indistinguishable from Castro et al.'s (2001) LFs, although small non-systematic differences occur due to the different methods used. We combined the LFs obtained from the three individual fields into a single background LF. The uncertainties due to possible background variations thus introduced are negligible compared to the errors in our source magnitudes, in particular for the fainter stars, where such background variations would be of importance (cf. Castro et al. 2001).

The LFs needed to be scaled to apply to the appropriate areas used to study the radial dependence of the cluster LFs, and subsequently subtracted from those. Since all of our background fields have longer exposure times than the longest CEN exposures, saturation sets in at brighter magnitudes than for these CEN fields. To correct for the background contribution at the brightest magnitudes, $V \leq V_{\rm sat.,bg}$, and $I \leq I_{\rm sat.,bg}$, we simply extrapolated the background field LFs to $V = V_{\rm sat.,short}$, and $I = I_{\rm sat.,short}$, i.e., to the brightest unsaturated stars in our short CEN exposures. The extrapolated number of background field stars brighter than the saturation limits of our background fields is negligible for practical purposes, however. In the remainder of this paper, when we refer to the cluster LFs, this applies to the background-corrected LFs.

Foreground stars are not a source of confusion in the

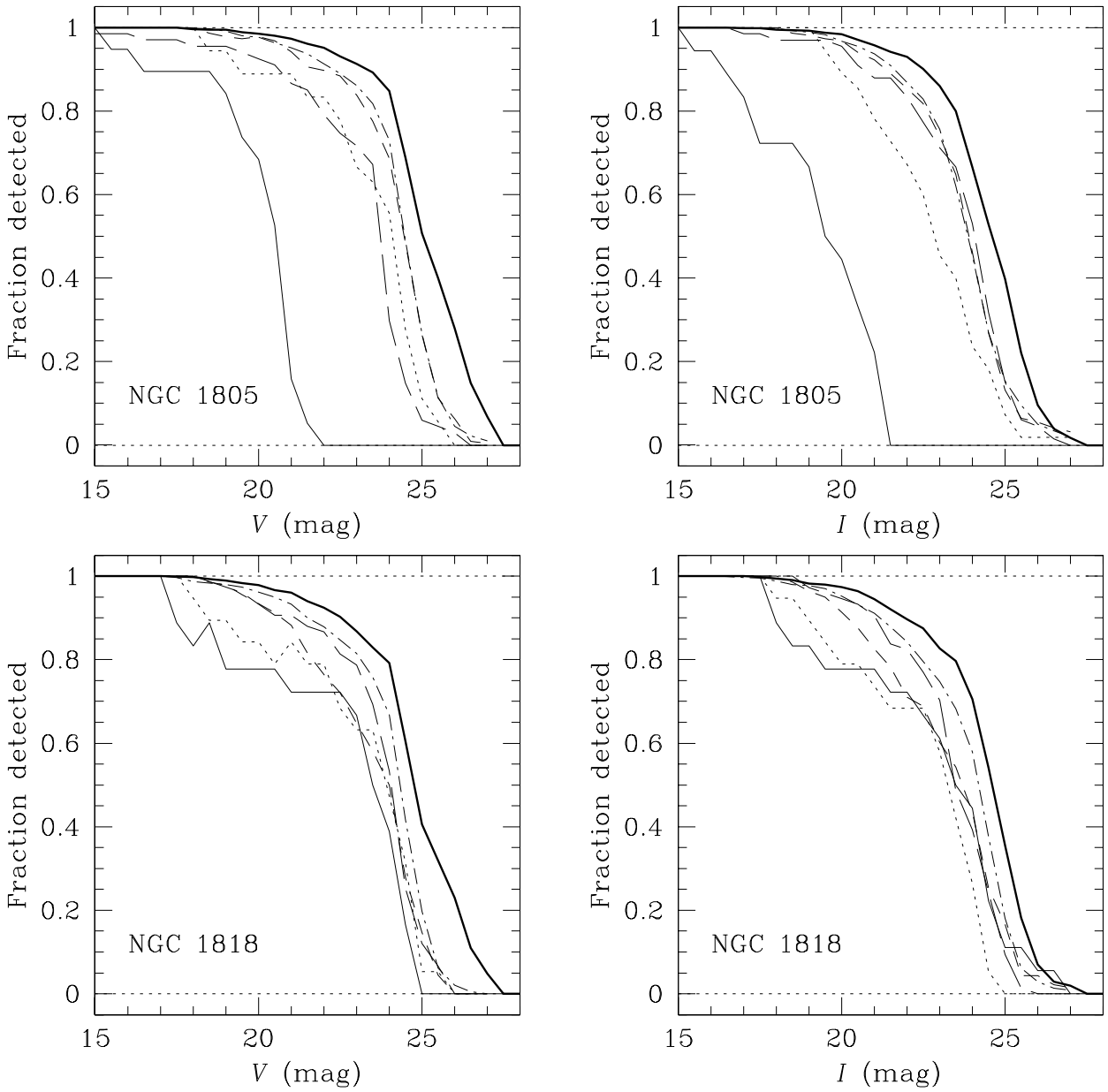


**Figure 2.** Completeness curves for NGC 1805 and NGC 1818. The different line styles refer to different annuli: thin solid – $r \leq 3.6''$ (NGC 1805: short exposures); dotted – $3.6'' < r \leq 7.2''$; long dashes – $7.2'' < r \leq 18''$; short dashes – $18'' < r \leq 36''$; dash-dotted – $36'' < r \leq 54''$; thick solid – $r > 54''$.

case of our LMC clusters. From careful inspection of the CMDs presented by Johnson et al. (2001), we conclude that for $V \lesssim 23$ there are most likely no foreground stars in our fields of view. This is consistent with the standard Milky Way star count models (e.g., Ratnatunga & Bahcall 1985).

### 3.1 Evidence for systematic luminosity segregation

Figs. 4 and 5 show the distribution of stellar magnitudes as a function of distance from the cluster centres. The shaded histograms represent the total number of stars in our final source lists, not corrected for incompleteness, area covered or background star contamination; the thick solid lines are the actual cluster star distributions, obtained by subtracting the background contribution expected in the area covered by

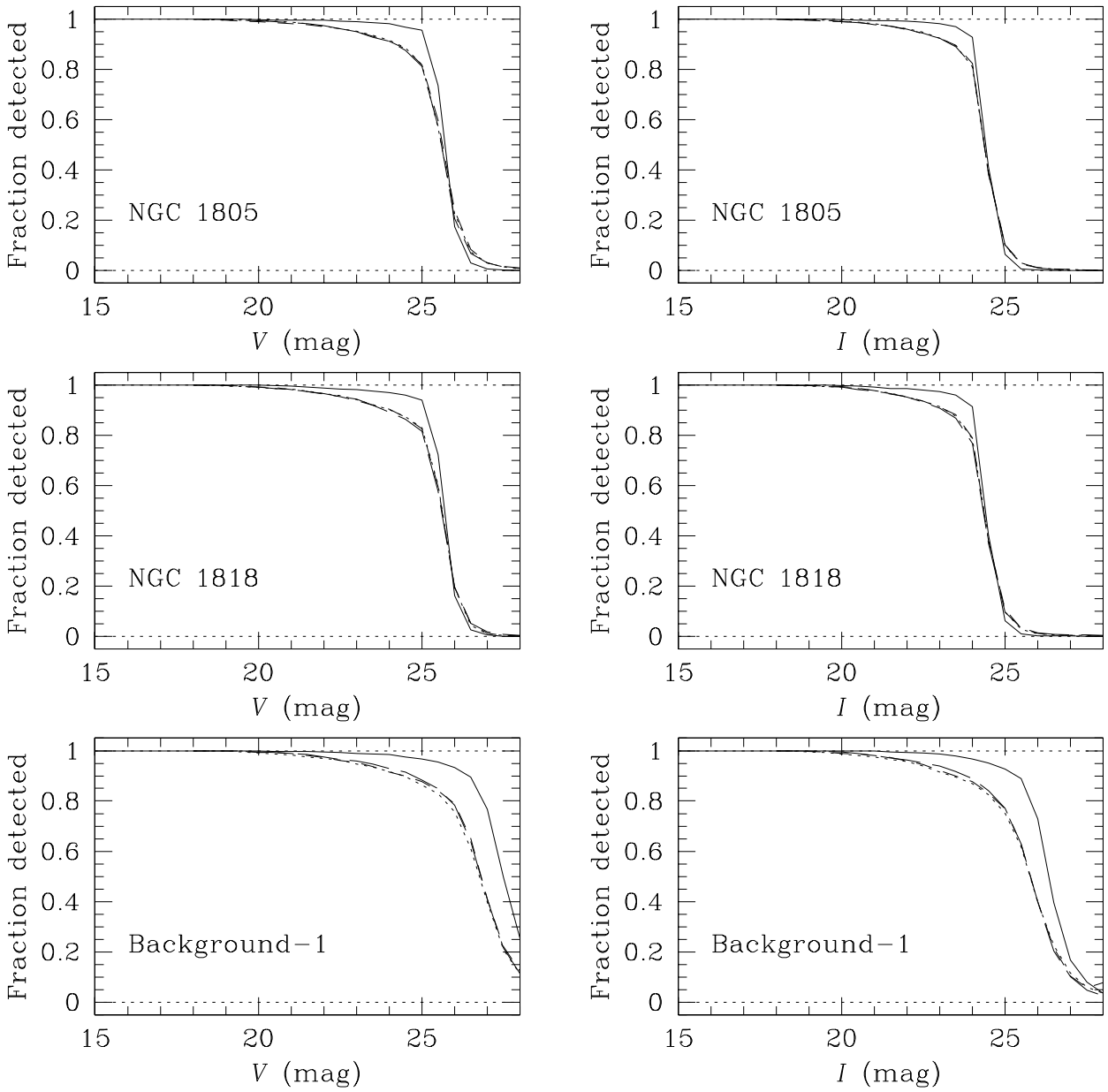


**Figure 3.** Completeness curves for the background fields. The different line styles refer to the individual *WFPC2* chips; the smaller pixel size of the PC chip (solid lines) clearly increases the completeness fraction; for the WF chips (dotted, long and short-dashed lines), a single completeness correction applies.

each annulus from the observed total LFs and subsequently correcting for incompleteness effects. The 50% completeness limits in each annulus are indicated by the vertical dashed lines through the centres of the last magnitude bin above this limit. We have used the $V$-band completeness curves to correct our LFs for the effects of incompleteness. However, since the final source lists of cluster stars were based on cross referencing the detections both in the $V$ and $I$ bands, we need to be careful close to the 50% completeness limit in $V$. Close examination of Fig. 2 shows that the $I$-band magnitude is always brighter than the corresponding $V$-band magnitude, for any completeness fraction. This affects the derived LFs in Fig. 4, in particular for $M_V \lesssim 2.7$ ($R \leq 7.2''$) and $M_V \lesssim 3.5$ ($7.2 < R \leq 14.4''$), so that any LF slope derived for these radial ranges and including stars within $\sim 1.5$ magnitude of the 50% completeness limit is a *lower* limit. This effect does not play a significant role for NGC 1818.

Secondly, for the inner radial bin ($R \leq 7.2''$) of NGC 1805 the incompleteness for the fainter stars is severe due to

the large concentration of bright stars in the very compact core of this cluster. Therefore, the declining LF for $M_V \gtrsim 1$ is likely due to the central incompleteness in this inner radial bin, and any LF slope derived for these stars will thus also be a lower limit.

The effects of strong luminosity segregation are clearly visible, in the sense that the brighter cluster stars are strongly concentrated in the inner $\sim 20''$ in each cluster. The brightest unsaturated cluster stars, i.e., $V \lesssim 17$, consist of a mixture of stars at the top of the main sequence and giant branch/red clump stars (cf. the CMDs in Johnson et al. 2001), which span only a very narrow mass range, while the fainter stars are main sequence stars. The effects are strongest in NGC 1805; strong luminosity segregation in this cluster was already apparent from an initial visual examination of Fig. 1.

In Figs. 6a and b we show all annular cluster LFs out to $R = 72.0''$, corrected for the effects of incompleteness (as a function of radial distance from the cluster centres), background contamination and for the sampling area covered by each (partial) annulus, for NGC 1805 and NGC 1818, respectively. In this representation, the radial dependence of the cluster LFs is more easily visible than in Figs. 4 and 5. For the NGC 1818 field, these annular LFs are not contaminated by the companion cluster NGC 1818 B, since the latter is located at larger radii than covered by our LFs. We also show the overall cluster LFs, constructed by adding all individual annular LFs weighted by the area covered by the observations. This procedure ensures the proper treatment of the sampling incompleteness at each annular radius. For NGC 1805 the completeness corrections of the innermost annulus (and to some lesser degree also of the second annulus) are uncertain due to severe crowding and statistical noise (small-number statistics), likely causes an artificial turndown for the lowest luminosities. However, the contribution of this annular LF to the overall LF is $\lesssim 5\%$, because of the weighting by area used in its construction, with the inner annulus covering only $\sim 1.7\%$ of the total area covered by our observations for $R \leq 72.0''$

In paper III we will extend the overall LFs down to the lowest-luminosity sources detected reliably in our STIS fields, for the entire LMC cluster sample. Our ultimate aim is to determine whether the cluster LFs – and thus their MFs – are statistically indistinguishable or significantly different over the entire mass range, down to the lowest masses. This forms part of our efforts to determine the strength of the apparent universality of the IMF.

We subsequently determined the LF slopes, assuming a simple power-law dependence, i.e., $N(L) \propto L^{-\alpha}$, where $\alpha$ is the LF slope (but see Sec. 4). Although we used the power-law approximation to be able to compare our results to previously published LF slopes, we realise that the inner LFs in Figs. 4 and 5 show a clear maximum inside our fitting ranges, and that the overall cluster LFs are clearly *not* linear. Despite this, a comparison of LF slopes obtained using power-law fits over identical luminosity ranges is still valuable to quantify the radial dependence of the cluster LFs, however. We chose to use fitting ranges in luminosity that covered the maximum overlap among our annular LFs in order to minimise the effects of small-scale statistical fluctuations in the LFs. For NGC 1805, we used the ranges $-2.2 \leq M_V \leq 4.2$ ($2.81 \geq \log(L_V/L_{V,\odot}) \geq 0.25$) for $R \leq 72.0''$ and the slightly greater common magnitude range $-2.2 \leq M_V \leq 5.0$ ($2.81 \geq \log(L_V/L_{V,\odot}) \geq -0.07$) for $7.2 < R \leq 72.0''$. The latter magnitude range was also used for fitting the LF slopes in NGC 1818, and is indicated by the vertical dashed fitting boundaries in Fig. 6. We note, however, that Johnson et al.'s (2001) CMDs show confusion by Be stars for $V \lesssim 17, M_V \lesssim -1.6$, so that our brightest data point needs to be taken with caution. This does not affect the overall results presented in this section, however. The error bars in the LF slopes include the formal error and the statistical uncertainties due to poisson noise.

In the top panels of Fig. 7 we show the dependence of the slope of the LF on cluster radius; the radial ranges to which the data points apply are indicated by small bars at the bottom of each panel.

We have also included the LF slopes from the STIS HALF field LFs (open squares), obtained following identical procedures as for the *WFPC2* $V$-band LFs. We used a fitting range to obtain the LF slope of $-1.0 \leq M_V \leq 5.0$ ($2.33 \geq \log(L_V/L_{V,\odot}) \geq -0.07$) for both of our single fields. The source distributions in our STIS fields peak at $58.4''$ and $44.2''$ for NGC 1805 and NGC 1818, respectively. Their radial extent is roughly 48 and $44''$, respectively (i.e., the FWHMs of the radial distributions). The fact that the STIS data points are entirely consistent with the *WFPC2* results, although they were determined completely independently and using a different detector, confirms the robustness of these results. For comparison, we have also indicated the LF slopes one would arrive at by taking the overall cluster LFs, indicated by "all".

Both clusters show clear evidence of luminosity segregation, in the sense that the LF slopes steepen with increasing cluster radius. In NGC 1805, the LF slopes reach a stable level beyond $\simeq 15''$ (or $\sim 3.8$ pc), well beyond the cluster's half-light radius at 1.8 pc. A stable LF slope is reached for $R \gtrsim 25''$ ($\sim 6.3$ pc) in NGC 1818, again indicating strong luminosity segregation in the inner annuli.

Although the trend towards steeper LFs with increasing radius is clear, the associated error bars are large. They are the formal errors from the fit of a single power law to the data points, and are therefore dominated by the non-linearity of the annular LFs and point-to-point variations. The non-linear behaviour of the annular LFs is also our preferred explanation for the $\sim 10\%$ difference in measured LF slopes for our two fitting ranges in luminosity used for NGC 1805. We will return to this issue in Sec. 4.

### 3.2 The brightest cluster stars

Finally, we can use the distribution of the saturated stars in the short CEN exposures to strengthen our conclusions on the presence of strong luminosity segregation in both clusters. Saturated stars in the short CEN exposures are brighter than 15.5, and 15.0 mag (in both $V$ and $I$) in NGC 1805 and NGC 1818, respectively. Fig. 8 shows the radial distribution of these brightest cluster members, in units of the clusters' half-light radii. We show the original star counts as the dashed histograms. However, to interpret these distributions in terms of mass segregation, we need to correct these for the underlying cluster surface brightness distribution. We assumed King-like cluster profiles of the form sug-

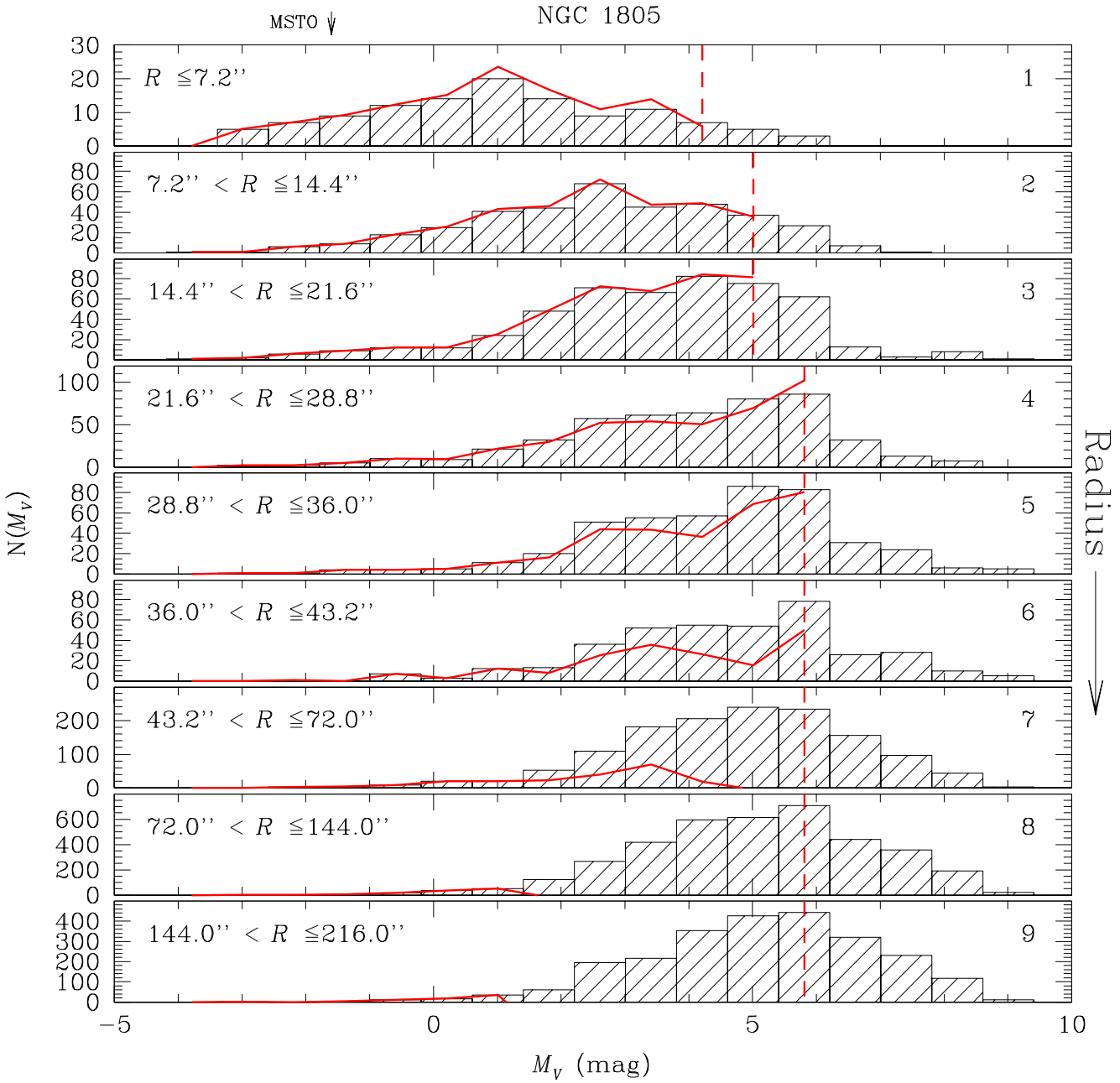


**Figure 4.** Observational total LFs from our *WFPC2* data in annuli at increasingly large radii from the NGC 1805 cluster centre (histograms). The thick solid lines are the actual cluster star distributions, after correction for the background field star contribution and the effects of incompleteness; the 50% completeness limits are indicated by the vertical dashed lines. The numbers on the right-hand side in each panel refer to the corresponding annular LFs in Fig. 6. The main sequence turn-off magnitudes ("MSTO") are indicated by the arrows.

gested by Elson et al. (1987) to obtain the corrected, shaded histograms.

We can firmly rule out a Galactic foreground origin for these sources, since the standard Milky Way models predict $\lesssim 0.005$ foreground stars to appear in an area corresponding to the PC field of view towards these clusters. There is clear evidence for luminosity segregation in both clusters, with a strong concentration of the brightest stars within the inner $\sim 4$ and $\sim 8R_{\rm hl}$ in NGC 1805 and NGC 1818, respectively. This result is largely independent of the radial bin size adopted.

### 3.3 Ejection of bright stars?

Following similar procedures as for the *WFPC2* observations, we obtained calibrated $V$ and $I$-band source lists for

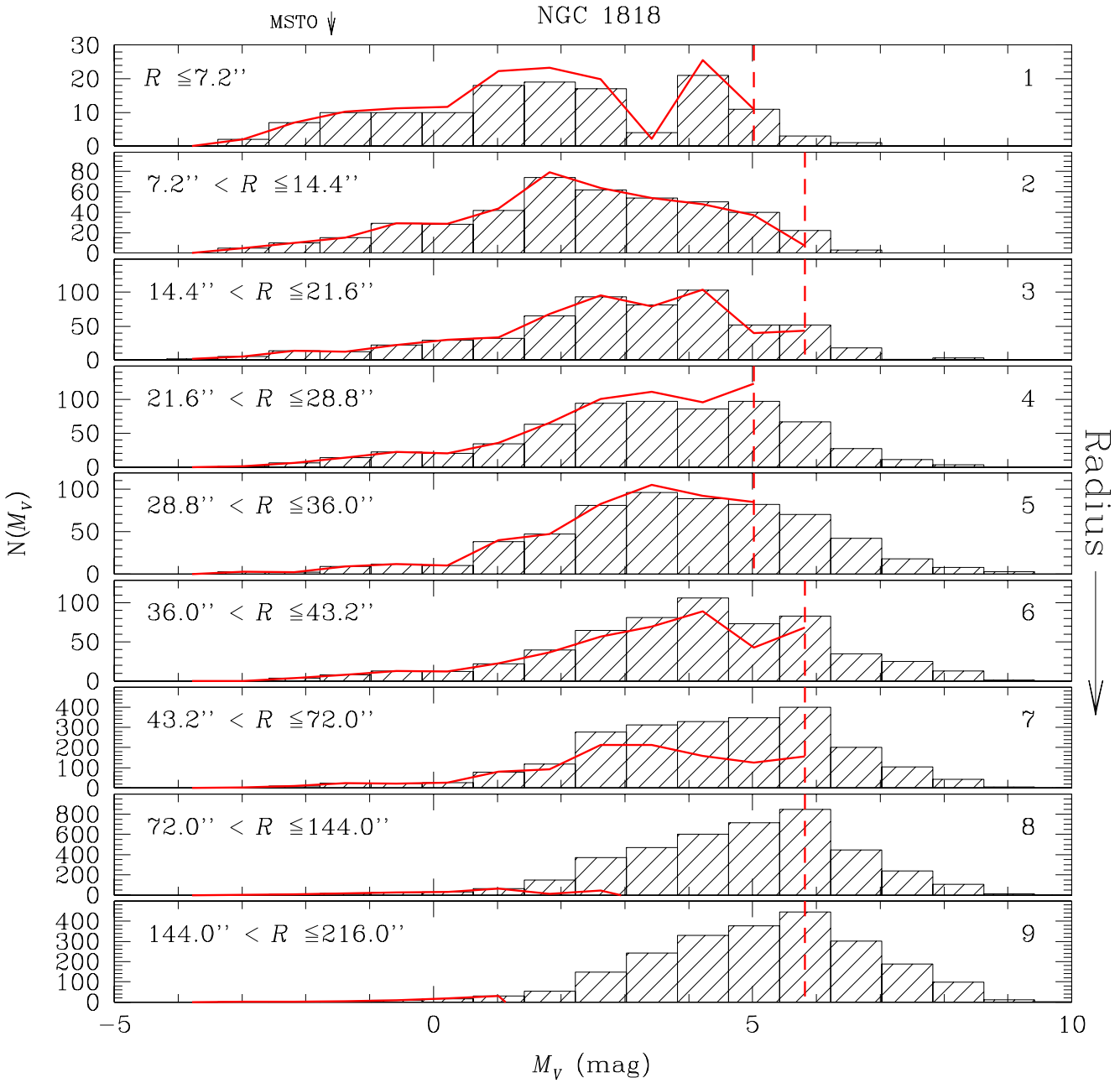


**Figure 5.** Same as Fig. 4, but for NGC 1818.

the wide-field NTT data. These observations were obtained to study the distribution of cluster (and field) stars near and above the main sequence turn-off, which occurs at $V \sim 17$ for both clusters. The magnitude range $15.5 \lesssim V \lesssim 20.0$ is available for the combined cluster and field star populations.

The main purpose of our use of the NTT fields was to establish whether there is evidence that a fraction of the brighter cluster stars have been ejected from the cluster on time-scales similar to the cluster ages, $\sim 10-25$ Myr. Therefore, we examined the radial distributions of the combined cluster+field star populations (centred on the cluster centres) for 0.5 mag bins, ranging from $V = 15.5$ to $V = 20.0$. Based on Figs. 4 and 5, we conclude that for radii $R \gtrsim 72.0''$ the LFs are dominated by the background field population. We will therefore conservatively focus our analysis of the NTT fields on radial 100 pixel ($27''$) bins beyond $R = 100''$, out to the edge of our fields of view at $\simeq 330''$. For stars fainter than $V \sim 17.5$, the numbers of stars as a function of radius, corrected for the area covered, are consistent with a flat distribution. This indicates that for these magnitude bins the observed stellar population is largely dominated by the background field. Therefore, we decided to use the radial distribution of stars in the magnitude range $18.5 \leq V \leq 19.5$ ($0 \lesssim M_V \lesssim 1$) as our control sample, to be used for the

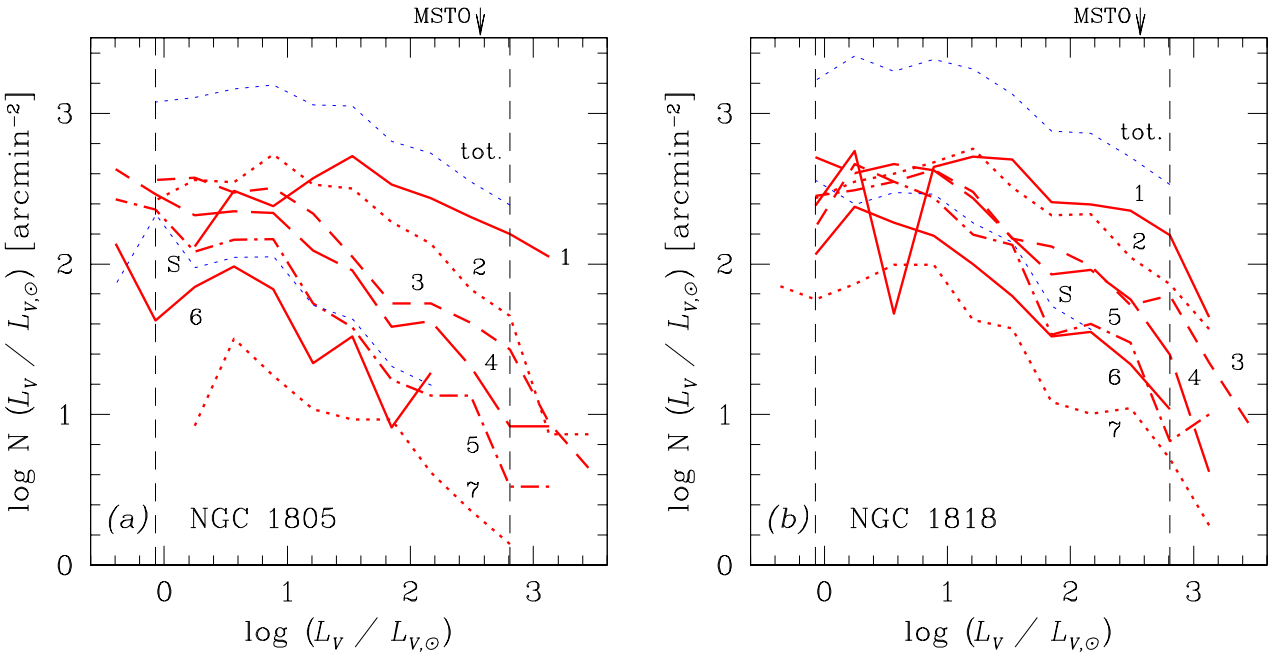


**Figure 6.** Luminosity functions in NGC 1805 and NGC 1818: comparison of annular LFs from the inner 7 annuli shown in Figs. 4 and 5 and the STIS HALF fields, normalised to 1 arcmin$^2$ area coverage. For reasons of clarity, we have omitted the vertical error bars. The dotted lines covering the range between the fitting boundaries (vertical dashed lines) and representing the largest numbers of stars / arcmin$^2$ are the overall cluster LFs. The annular bins are numbered as in Figs. 4 and 5, and represented by the following line styles (inside outwards), from top to bottom: solid, dotted, short dashed, long dashed, dot-dashed, dotted (STIS HALF fields, "S"), solid, and dotted. The approximate main sequence turn-off ("MSTO") luminosities are indicated by the arrows.

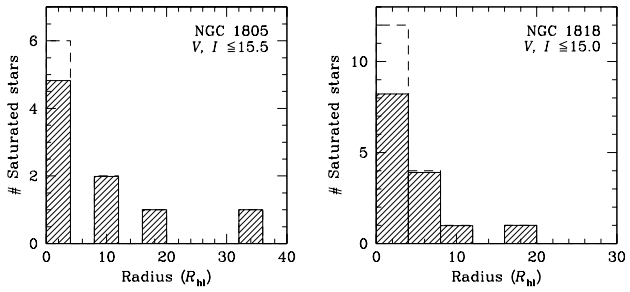


**Figure 8.** Radial distributions of the brightest (saturated) stars in NGC 1805 and NGC 1818; dashed histogram: original star counts, shaded histograms: corrected for the clusters' surface brightness distribution, as described in the text.

normalisation of the brightest magnitude ranges. At fainter magnitudes, one needs to take significant incompleteness corrections into account.

Although the numbers of bright stars in each of our fields are small (up to several tens in each 0.5 mag bin, for the entire radial range from $100'' - 330''$), for NGC 1818 there appears to be an excess of $\sim 8-10\%$ of brighter stars (i.e., an excess of $18 \pm 8$ stars of $15.5 \leq V \leq 16.0$, as well as brighter, saturated stars) towards the inner radial cut-off at $100''$ compared to the control sample. Because of the relatively small numbers of bright stars, and the associated statistical uncertainties, this is a $\sim 2\sigma$ result. This over-density is consistent with a radially decreasing distribution, suggesting that these bright stars are associated with NGC 1818. We will discuss the implications of this in terms of formation scenarios or dynamical ejection from the cluster core in Sec. 4.3.

For stars with magnitudes $V > 16.5$ in NGC 1818 and for the entire range in magnitudes for NGC 1805, the radial distributions are consistent with randomly distributed stars in the field, again compared to our control sample, $18.5 \leq V \leq 19.5$.

Finally, for the NTT field of view used for this analysis ($540'' \times 509''$), the Galaxy models of Ratnatunga & Bahcall (1985) predict roughly 14 foreground stars in the range $15 \leq V \leq 17$. Our samples contain at least twice as many stars in this magnitude range, for either field. In addition, if a significant fraction of the stars in this magnitude range were Galactic foreground stars, they would not be expected to be concentrated on the clusters, as found for NGC 1818.

## 4 DISCUSSION

### 4.1 Comparison with previously published results

In this section, we compare our results to those of SBJG to illustrate the sensitivity of a simple single-parameter fit of an LF to star count data for compact star clusters. All of the adopted luminosity range, radial range, completeness range, and background subtraction affect an apparently robust result.

Since SBJG's published annular LF slopes were determined over a different magnitude fitting range than ours,

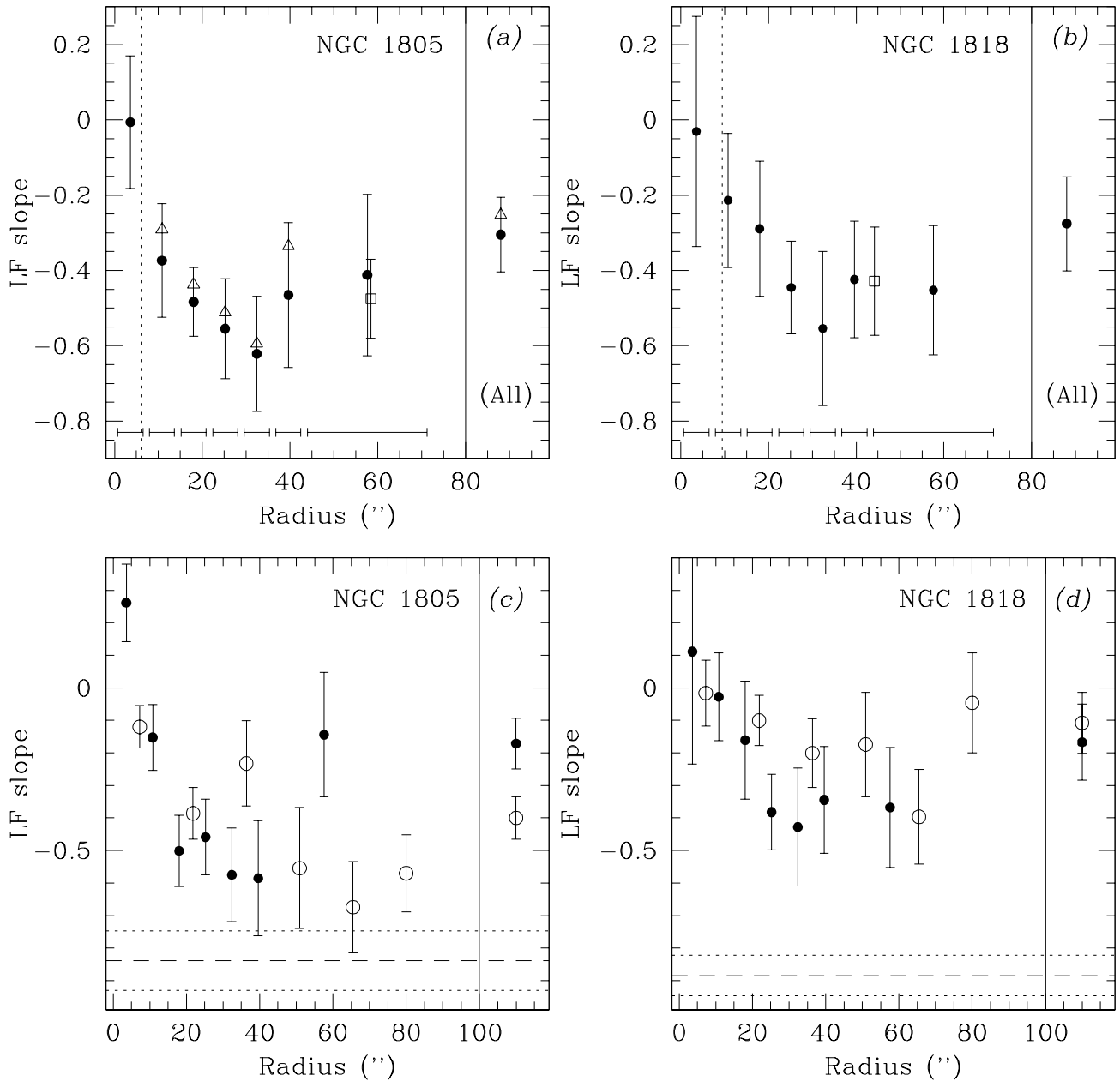


**Figure 7.** The dependence of the LF slope on the fitting range. *(a)* and *(b)* LF slopes determined between the fitting boundaries indicated in Fig. 6. (NGC 1805: the filled circles and error bars represent the smaller luminosity range, which could be applied to the entire radial cluster distribution; the open triangles were obtained by using the greater range in luminosity). We have also indicated the slope one would measure based on the overall cluster LFs (right-hand subpanels), and the slope obtained from the STIS HALF field CLFs (open squares). The vertical dotted lines indicate the cluster core radii. Comparison of our LF slopes with published in the literature. *(c)* and *(d)* – Comparison with SBJG after redetermination of the LF slopes using identical absolute magnitude ranges for each sample. Black dots: this paper, open circles: SBJG. The horizontal dashed and dotted lines represent the sky background level and its 1-$\sigma$ uncertainty, respectively, as discussed in the text.

we redetermined the slopes for both our LFs and those of SBJG over the common magnitude range $0.25 \leq M_V \leq 4.25$ ($1.83 \geq \log(L_V/L_{V,\odot}) \geq 0.23$), after converting SBJG's *WFPC2* flight system magnitudes to the standard *V*-band system. The results are shown in Figs. 7c and d, where the black dots represent the slopes determined from the LFs derived in this paper and the open circles are those from SBJG's published figures. The right-hand subpanels show the LF slopes if we had considered the entire stellar distribution of the clusters at once. We observe reasonable con-

sistency between our results, within the associated fitting uncertainties, although a small discrepancy is seen in the outer regions, beyond $R \simeq 50''$ for NGC 1805 and $R \simeq 70''$ for NGC 1818. Small differences between the overall cluster LFs of NGC 1805 could be explained by the fact that we used a radial range $R \leq 72.0''$, while SBJG's overall LF is based on the cluster members out to $R = 102.0''$.

Although the consistency between both our results is encouraging, in particular since they were obtained entirely independently, this comparison shows clearly that (annular) cluster LFs obtained at large distances from the cluster centre are significantly affected by small differences in the treatment of the background field star confusion and are therefore highly uncertain. In order to estimate the effect of background confusion, we determined the LF slope, using identical absolute magnitude ranges as for the cluster LFs (corrected for incompleteness), for our two radial bins at radii $R > 72.0''$ to investigate this effect. The resulting LF slopes for the background LMC stars are shown in Figs. 7c and d as the dashed lines with their associated 1-$\sigma$ uncertainties at the bottom of these panels.

Thus, we conclude that the value derived for the LF slope is critically dependent on the range in (absolute) magnitude (or luminosity) used for the fitting. However, if done consistently for the entire cluster sample, for all radial annuli, the relative variations among LF slopes as a function of radius are more robust.

Finally, Hunter et al. (1997) converted their *WFPC2* annular LFs of NGC 1818 into their associated MFs, but did not find evidence for mass segregation in this cluster for stellar masses in the range $0.85 \leq m \leq 9M_{\odot}$. However, they noted that the cluster core contains brighter stars that were not included in their study due to saturation, whereas the outer regions do not. The exposure times of their short-exposure F555W images are four times as long as those of our short exposures, resulting in a significantly greater fraction of saturated stars in their images. Therefore, we believe that the difference between our and their results is largely due to this saturation effect. Unfortunately, they did not publish background and incompleteness corrected LFs, so that we cannot directly compare our results. In paper II we will discuss these differences in more detail based on a comparison of the cluster MFs.

### 4.2 Is there a representative cluster radius?

Because of the sensitivity of the LF slope to the adopted luminosity and radial range and to the accuracy of the corrections for incompleteness and background star contamination of single power law fits to the annular LFs, we introduce a more robust characterisation of the presence of luminosity segregation in the NGC 1805 and NGC 1818 in Fig. 9. To minimise the sensitivity of the LF slope to these effects, we decided to quantify the deviations of the high-luminosity range of the annular LFs from the global LF. All annular LFs were normalised to the global LF in the range $-0.1 \leq \log(L_V/L_{V,\odot}) \leq 1.0$; subsequently, we determined the average sum of the differences between the global and the scaled annular LFs in the common luminosity range $1.0 < \log(L_V/L_{V,\odot}) \leq 2.57$ ($\log(L_V/L_{V,\odot}) \simeq 2.57$ corresponds to the main sequence turn-off), $\Sigma_{\rm red}\Big(\Delta \log N(L_V/L_{V,\odot})\Big)$.

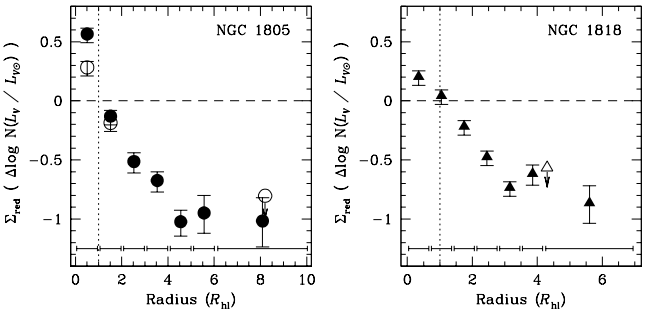


**Figure 9.** Deviations of the annular LFs from the global LF as a function of radius, as discussed in the text. The filled symbols represent the *WFPC2* data of NGC 1805 and NGC 1818, respectively; the open symbols at large radii are their STIS counterparts, which are upper limits due to the observed curvature of the LFs (see text). The error bars are dominated by statistical fluctuations in the LFs due to poisson noise. The horizontal bars at the bottom of the figure indicate the radial range used to obtain the data points; the vertical dotted lines represent the clusters' half-light radii.

The result for the inner two radial bins of NGC 1805 are upper limits due to the severe incompleteness effects for low-luminosity stars in its centre (cf. Section 3.1). In order to constrain these upper limits to their most likely range, we decided to adopt the shape of the third annulus ($14.4'' < R \leq 21.6''$) matched to the number counts of the inner annulus in the luminosity range $1.5 \leq \log L_V/L_{V,\odot} \leq 1.9$ as a conservative estimate of the "true" inner LFs – based on the robust assumption of no luminosity segregation for $\log L_V/L_{V,\odot} \leq 1.0$ at $R \sim 18'' = 1.53R_{\rm hl}$ – and repeated the above procedure for the inner two annuli. The resulting data points are shown as open symbols. Since the STIS LFs do not reach the brightest luminosity cut-off, we were forced to use a smaller fitting range; the resulting STIS data points are therefore upper limits, since the LFs are curved and not single power laws.

From Fig. 9, it is immediately clear that both clusters are luminosity segregated to at least $R \simeq 3 - 4R_{\rm hl}$, beyond which radius the deviations become relatively constant with increasing radius. Although it appears that the global cluster LF is fairly well approximated by half-light LF ($\simeq R_{\rm core}$ for these young clusters), the LFs at these radii are not representative of the dominant cluster stars, but are dominated by the segregated high-luminosity stars. In Paper III we will address this issue in more detail for our larger LMC cluster sample, for which we will investigate whether the cluster age affects the radius at which the local LF becomes representative of the cluster population as a whole.

### 4.3 Dynamical evolution on short time-scales?

In Sec. 3.3 we presented evidence for a marginal excess of bright stars ($V \leq 16.0$), corresponding to the most massive unsaturated stars in our LFs (see Paper II), surrounding NGC 1818 compared to the expected number of stars in the background field. For NGC 1805, our results are inconclusive.

It is unlikely that they originated independently from

the cluster in the background field. Although the LMC background field shows significant density contrasts, including in our NTT fields, the bright stars are not preferentially located in any of these. In particular, only 1 or 2 of them are located in the NGC 1818 B subcluster, while none of them seem to be associated with the open cluster-like object at $\sim 360''$ to the North West of the cluster centre.

Therefore, they are most likely massive stars that have been collisionally ejected from the cluster core due to encounters with other massive stars or binary systems. Although standard two-body interactions involving equal mass objects are not expected to eject a significant number of stars over the short lifetime of NGC 1818, unequal mass encounters, primordial mass segregation and – in particular – the presence of hard binaries can have a significant effect on the dynamical ejection of massive stars on short time-scales (e.g., Leonard & Duncan 1988, 1990, Leonard 1995, Portegies Zwart et al. 1999, Hoogerwerf, de Bruijne & de Zeeuw 2000, Brandl et al. 2001). In addition, the dynamical relaxation time of massive stars can be significantly shorter than that of low-mass stars (cf. Portegies Zwart et al. 1999).

Thus, this interpretation suggests that the cores of massive young star clusters undergo significant dynamical evolution, even on time-scales as short as $\sim 25$ Myr. A more extreme example of the dynamical evolution in the core of a very young star cluster was recently presented for the $\lesssim 3-4$ Myr old core of 30 Dor, R136 (Brandl et al. 2001).

In Paper II we will explore this issue in more detail; we will convert our LFs into the associated MFs and discuss the implications of the observed mass segregation in the context of mass segregation at birth versus that due to dynamical evolution.

## 5 SUMMARY AND CONCLUSIONS

In this paper, we have presented a detailed analysis of *HST/WFPC2* and STIS imaging observations, and of supplementary wide-field ground-based observations obtained with the NTT of two young ($\sim 10-25$ Myr) compact star clusters in the LMC, NGC 1805 and NGC 1818.

In principle, rich compact LMC star clusters are ideal laboratories for providing strong constraints on the universality of the IMF, in particular because they are essentially single-age, single-metallicity systems for which individual stars over a range of masses can easily be resolved. However, in order to understand the cluster IMF, a detailed knowledge of the presence and the effects of mass segregation is required. Observations of various degrees of mass segregation in very young star clusters suggest that at least some of this effect is related to the process of star formation itself.

In this paper, we have focussed on the analysis of the behaviour of the stellar LF as a function of radius in these two young LMC clusters; in Paper II, we will derive the associated MFs and discuss alternative diagnostics to quantify mass segregation effects, such as the dependence of cluster core radius on the adopted mass (or luminosity) range.

Although the effects are strongest in NGC 1805, the more strongly concentrated cluster, we present clear evidence for strong luminosity segregation in both clusters:

(i) The brighter cluster stars are strongly concentrated in the inner $\sim 3-4R_{\rm hl}$ in each cluster. Compared to the outer cluster regions, the fainter stars in the central annuli are significantly underpopulated relative to the brighter stars.

(ii) The LF slopes steepen with cluster radius. In both clusters, the LF slopes reach a stable level well beyond the clusters' half-light radii.

(iii) The brightest, saturated cluster stars ($V, I \lesssim 15.5$ and 15.0 for NGC 1805 and NGC 1818, respectively) are predominantly located within the inner $\sim 4-8R_{\rm hl}$.

From a detailed analysis of the shape of the LF, we show that the value derived for the LF slope is critically dependent on the range in (absolute) magnitude (or luminosity) used for the fitting.

Finally, from the wide-field NTT observations we present tentative evidence for the presence of bright stars surrounding NGC 1818 which we argue to be associated with the cluster. We suggest that they are most likely massive stars that have been collisionally ejected from the cluster core due to unequal-mass encounters, primordial mass segregation or collisions with (hard) binary systems. This interpretation leads us to suggest, therefore, that the cores of massive young stars clusters undergo significant dynamical evolution, even on time-scales as short as $\sim 25$ Myr.

## ACKNOWLEDGMENTS

This paper is based on observations with the NASA/ESA *Hubble Space Telescope*, obtained at the Space Telescope Science Institute, which is operated by the Association of Universities for Research in Astronomy (AURA), Inc., under NASA contract NAS 5-26555. We thank the ESO Data Flow Operations Team for carrying out our NTT service observations, in particular Massimo Ramella and Bruno Leibundgut. We also thank Dougal Mackey for his assistance. We acknowledge insightful and constructive comments by the referee. This research has made use of NASA's Astrophysics Data System Abstract Service.

## REFERENCES

Andreuzzi G., De Marchi G., Ferraro F.R., Paresce F., Pulone L., Buonanno R., 2001, A&A, 372, 851

Beaulieu S.F., Elson R.A.W., Gilmore G.F., Johnson R.A., Tanvir N., Santiago B.X., 1999, in: New Views of the Magellanic Clouds, IAU Symp. 190, Chu Y.-H., Suntzeff N., Hesser J., Bohlender D., eds., Victoria, Canada, p. 460

Beaulieu S.F., Gilmore G.F., Elson R.A.W., Johnson R.A., Santiago B.X., Sigurdsson S., Tanvir N., 2001, AJ, 121, 2816

Brandl B., Chernoff D.F., Moffat A.F.J., 2001, in: "Extragalactic Star Clusters", IAU Symposium 207, Pucón (Chile), March 2001, eds. Grebel E.K., Geisler D., in press

Brandl B., Sams B.J., Bertoldi F., Eckart A., Genzel R., Drapatz S., Hofmann R., Löwe M., Quirrenbach A., 1996, ApJ, 466, 254

Caloi V., Cassatella A., 1998, A&A, 330, 492

Campbell B., et al., 1992, AJ, 104, 1721

Carpenter J.M., Meyer M.R., Dougados C., Strom S.E., Hillenbrand L.A., 1997, AJ, 114, 198

Cassatella A., Barbero J., Brocato E., Castellani V., Geyer E.H., 1996, A&A, 306, 125

Castro R., Santiago B.X., Gilmore G.F., Beaulieu S., Johnson R.A., 2001, MNRAS, 326, 333

Da Costa G.S., 1982, AJ, 87, 990

de Grijs R., Gilmore G.F., Johnson R.A., Mackey A.D., 2001, MNRAS, submitted (Paper II)
de Grijs R., O'Connell R.W., Gallagher J.S., 2001, AJ, 121, 768
Elson R.A.W., Fall S.M., 1988, AJ, 96, 1383
Elson R.A.W., Fall S.M., Freeman K.C., 1987, ApJ, 323, 54
Elson R.A.W., Freeman K.C., Lauer T.R., 1989, ApJ, 347, 69
Elson R.A.W., Sigurdsson S., Davies M.B., Hurley J., Gilmore G.F., 1998, MNRAS, 300, 857
Elson R.A.W., Tanvir N., Gilmore G.F., Johnson R.A., Beaulieu S.F., 1999, in: New Views of the Magellanic Clouds, IAU Symp. 190, Chu Y.-H., Suntzeff N., Hesser J., Bohlender D., eds., Victoria, Canada, p. 417
Fischer P., Pryor C., Murray S., Mateo M., Richtler T., 1998, AJ, 115, 592
Grebel E.K., 1997, A&A, 317, 448
Harris W.E., Canterna R., 1980, ApJ, 239, 815
Hillenbrand L.A., 1997, AJ, 113, 1733
Hillenbrand L.A., Carpenter J.M., 2000, ApJ, 540, 236
Hillenbrand L.A., Hartmann L.E., 1998, ApJ, 492, 540
Holtzman J.A., et al., 1995a, PASP, 107, 156
Holtzman J.A., Burrows C.J., Casertano S., Hester J.J., Trauger J.T., Watson A.M., Worthey G., 1995b, PASP, 107, 1065
Hoogerwerf R., de Bruijne J.H.J., de Zeeuw P.T., 2000, ApJ, 544, L133
Houdashelt M.L., Wyse R.F.G., Gilmore G.F., 2001, PASP, 113, 49
Hunter D.A., Light R.M., Holtzman J.A., Lynds R., O'Neil E.J., Grillmair C.J., 1997, ApJ, 478, 124
Hunter D.A., Shaya E.J., Holtzman J.A., Light R.M., O'Neil E.J., Lynds R., 1995, ApJ, 448, 179
Johnson R.A., Beaulieu S.F., Gilmore G.F., Hurley J., Santiago B.X., Tanvir N.R., Elson R.A.W., 2001, MNRAS, 324, 367
Kontizas M., Hatzidimitriou D., Bellas-Velidis I., Gouliermis D., Kontizas E., Cannon R.D., 1998, A&A, 336, 503
Krist J., Hook R., 1997, The Tiny Tim User's Guide, version 4.4
Lada E.A., DePoy D.L., Evans N.J., Gatley I., 1991, ApJ, 371, 171
Leonard P.J.T., 1995, MNRAS, 277, 1080
Leonard P.J.T., Duncan M.J., 1988, AJ, 96, 222
Leonard P.J.T., Duncan M.J., 1990, AJ, 99, 608
Larson R.B., 1993, in: The Globular Cluster–Galaxy Connection, Smith G.H., Brodie J.P., eds., ASP Conf. Ser. 48, San Francisco: ASP, p. 675
Malumuth E.M., Heap S.R., 1994, AJ, 107, 1054
Mateo M., Hodge P., 1986, ApJS, 60, 893
Mateo M., Hodge P., 1987, ApJ, 320, 626
Mateo M., Hodge P., Schommer R.A., 1986, ApJ, 311, 113
Nemec J.M., Harris H.C., 1987, ApJ, 316, 172
Papenhausen P., Schommer R.A., 1988, in: The Harlow Shapley Symposium On Globular Cluster Systems in Galaxies, Grindlay J., Philip A.G.D., eds., IAU Symp. 126, Dordrecht: Kluwer, p. 565
Paresce F., De Marchi G., Jedrzejewski R., 1995, ApJ, 442, L57
Portegies Zwart S.F., Makino J., McMillan S.L.W., Hut P., 1999, A&A, 348, 117
Ratnatunga K.U., Bahcall J.N., 1985, ApJS, 59, 63
Rieke G.H., Lebofsky M.J., 1985, ApJ, 288, 618
Santiago B.X., Beaulieu S., Johnson R., Gilmore G.F., 2001, A&A, 369, 74 (SBJG)
Santos Jr. J.F.C., Bica E., Claría J.J., Piatti A.E., Girardi L.A., Dottori H., 1995, MNRAS, 276, 1155
Saviane I., Piotto G., Fagotto F., Zaggia S., Capaccioli M., Aparicio A., 1998, A&A, 333, 479
Shara M.M., Drissen L., Bergeron L.E., Paresce F., 1995, ApJ, 441, 617
Sirianni M., Nota A., De Marchi G., Leitherer C., Clampin M., 2001, in: "Extragalactic Star Clusters", IAU Symposium 207, Pucón (Chile), March 2001, eds. Grebel E.K., Geisler D., in press
Stetson P.B., 1987, PASP, 99, 91
Subramaniam A., Sagar R., Bhatt H.C., 1993, A&A, 273, 100
Testi L., Palla F., Prusti T., Natta A., Maltagliati S., 1997, A&A, 320, 159
Westerlund B.E., 1961, Uppsala Astr. Obs. Ann., 5(1)
Whitmore B., Heyer I., Casertano S., 1999, PASP, 111, 1559
Will J.-M., Bomans D.J., Tucholke H.-J., de Boer K.S., Grebel E.K., Richtler T., Seggewiss W., Vallenari A., 1995, A&AS, 112, 367